University of Southern Queensland

Faculty of Engineering and Surveying

Predicting the Crushing Stress of Composite Materials

A dissertation submitted by

Ang Soon Lim

in fulfillment of the requirements of

Courses ENG4111 and 4112 Research Project

towards the degree of

Bachelor of Mechanical Engineering

Submitted: November, 2006

Abstract

A simple mathematical model for predicting the crushing stress of the composite materials is presented in this report. The present knowledge of fracture mechanics and strength of materials are used as a basis for the modeling process.

The fracture mechanics part of analysis was based on the energy release rate approach. The energy release rate (G) of the proposed model was determined by this approach. This energy release rate was based on the Mode 1 (opening or tensile mode) failure. As for the strength of materials part of analysis, buckling theory was used to determine the critical load of the fibre beams.

These two engineering concepts were combined to form the equation for the proposed model. The derived equation should be a function of the materials properties, geometric and physical parameters of the composite materials.

The calculated stresses from the derived equation were compared with experimental data from technical and research papers. Good agreements shown in the results are encouraging and recommendations for future analysis with different modes of failure were also presented.

Acknowledgment

I wish to thank the following for their support and encouragement given to me throughout this project:

1. Dr Harry Ku, my supervisor and Mr Steven Goh, my Co-supervisor, for their invaluable support and encouragement throughout the project.
2. Ms Seah Jeng May, my wife, for her patience and encouragement.

University of Southern Queensland

Faculty of Engineering and Surveying

ENG4111 & ENG4112 *Research Project*

Limitations of Use

The Council of the University of Southern Queensland, its Faculty of Engineering and Surveying, and the staff of the University of Southern Queensland, do not accept any responsibility for the truth, accuracy or completeness of material contained within or associated with this dissertation.

Persons using all or any part of this material do so at their own risk, and not at the risk of the Council of the University of Southern Queensland, its Faculty of Engineering and Surveying or the staff of the University of Southern Queensland.

This dissertation reports an educational exercise and has no purpose or validity beyond this exercise. The sole purpose of the course pair entitled "Research Project" is to contribute to the overall education within the student's chosen degree program. This document, the associated hardware, software, drawings, and other materials set out in the associated appendices should not be used for any other purpose: if they are so used, it is entirely at the risk of the user.

Prof G Baker
Dean
Faculty of Engineering and Surveying

Certification

I certify that the ideas, designs and experimental work, results, analyses and conclusions set out in this dissertation are entirely my own effort, except where otherwise indicated and acknowledged.

I further certify that the work is original and has not been previously submitted for assessment in any other course or institution, except where specifically stated.

Ang Soon Lim

Student Number: 0031132352

_____
Signature

_____
Date

Table of Contents

Chapter 1

Introduction

1.1 Background

Composite materials have played an important role in achieving overall performance improvements in advanced structure. However, these benefits are often limited by premature damage in the form of fracture and delamination. Since structures consisting of composite members are getting larger and more complex, the joining of several structural members is becoming more and more common, and design is more often dictated by the structural joint strength.

Joining by mechanical fasteners is a common technology for assembling structural components in the aerospace and automobile industries. It is well known that fasteners can severely reduce the load bearing capacity of the composite materials by more than fifty percent. Due to anisotropy and inhomogenity of composite materials, the failure and strength of bolted composite joints can be considerably different from the failure and strength of metallic joints. Damage in bolted composite joints can initiate, at an early loading stage, and accumulate inside the composite materials as the load increases. This accumulation and failure mode strongly depend on the material, ply orientation, laminate thickness, joint geometry and loading conditions, etc.

There are three basic joint failure modes related to composite joints: net tension, shear out and bearing. Joint failures with the first two modes are catastrophic resulting from excessive tensile and shear stresses. However bearing damage is progressive and is related to compressive failure.

1.2 Objective

The objective of this project is to model the bearing failure of the composite joint with that of progressive crushing. To model the crushing stress model, two engineering concepts were used, fracture mechanics and strength of the materials. The energy release rate approach of linear elastic fracture mechanics was used to develop the energy release rate (G) of the model. Using the buckling theory of mechanics of materials, the critical load (P_{cr}) can be found for the fibre strand.

Combining these two concepts, the crushing stress therefore can be derived. The derived equation should be closed form and is a function of the following properties or parameters.

G	-	Energy release rate of the laminate
E	-	Modulus of the laminate in the transverse direction
θ	-	Crack opening angle in degree
h	-	Thickness of the composite
a	-	Crack length

Therefore in a generalized mathematical form, the crushing stress is

$$\sigma_c = f(G, E, \theta, h, a)$$

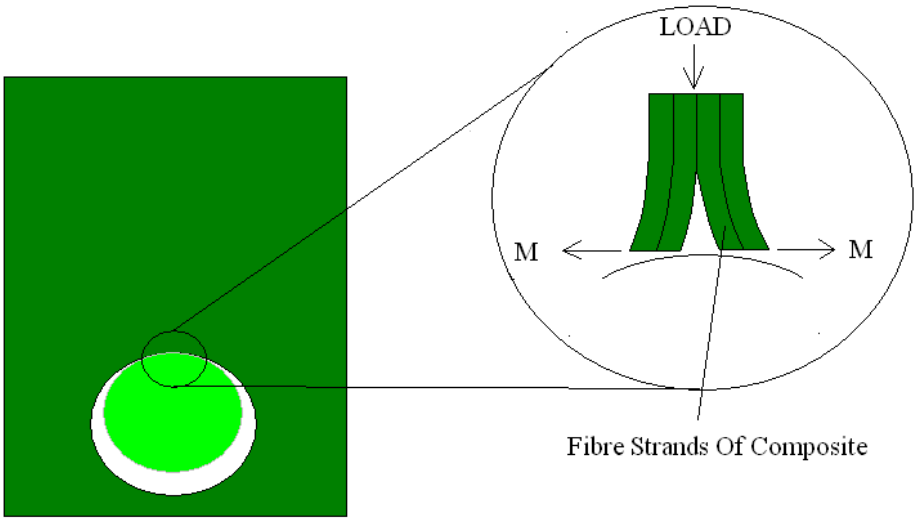

Figure 1.1 : General Model Representation

The diagram in figure 1.1 illustrates the general representation of the model.

Chapter 2

Literature Review

2.1 Review of Previous Works on Crushing Behaviour and Specific Energy Abortion

Composite materials, because of their inherent flexibility in their design for improved materials properties, have wide application in the automobile and aerospace industries. However their failure mechanism is highly complicated and rather difficult to analyze.

Farley [1] studied the effect of crushing speed on the energy absorbing characteristic of kelvar/epoxy and graphite/epoxy tubes and found that for graphite/epoxy tubes with [0±θ] fibre orientation, the specific energy did not vary with the crushing speed but the reverse were true for [±θ] fibre orientation. In kelvar/epoxy tubes, however, the energy absorption capacity increases with speed in all cases considered.

Further studies were carried out by Farley and Jones [2] to find the specific energy for different ply orientation and geometries of kelvar/epoxy and graphite/epoxy tubes. A commercially available non-linear FEM program (EAL – Engineering Analysis Language) was used for this purpose. For the kelvar/epoxy tubes the program predicted an energy absorption capability slightly increase between θ=15˚ and 45˚ and decreases between θ=45˚ and 75˚. This finding is 25 percent higher than the experimental results. For the graphite/epoxy tubes, the predicted energy absorption capability is highest at θ=15˚ and decreases in a near

linear manner as θ increases. The predicted value is 28 percent higher than experimental values at θ=15˚ whereas at θ=75˚ the predicted values is 22 percent of the experimental value. The agreement between analytical and experimental suggests that the important phenomena of the crushing process have been included in the model.

Thornton [3] studied the behaviour of various fibre reinforced plastic (FRP) tubes (glass, graphite and Kevlar fibres with epoxy resin) for different lay-ups and thickness to diameter ratios and showed that the specified energy absorption of FRP tubes was higher than some of the high tensile metallic tubes. Thornton used a 45º chamfer at one end of each tube to initiate the deformation, irrespective of the fibre orientation and lay-up in the tubes. He discovered that all the tubes collapsed by disintegration except the 45/-45 kelvar /epoxy tubes, which collapsed by buckling like metal tubes and specific energy absorption of the tubes was found to be less sensitive to thickness and diameter ratios than in the case of metal tubes.

Further experiments were carried out by Edwards [4] on kelvar, graphite and glass fibre with epoxy resin on rectangular, square and round cross sections. He observed that specimens of planar section were less effective in energy absorption than the circular sections.

Fairfull and Hull [5] carried out experiments to study the frictional energy involved in crushing of composite tubes between platens with different roughness values and classified different factors that contribute to the energy dissipation of

the tubes. They concluded that on a standard testing machine, the coefficient of friction, μ, is equal to 0.35.

Reddy and Wall [6] investigated the effect of foam filling on the energy absorption capability of sheet metal tubes in both static and dynamic axial compression and found that the mode of deformation during collapse changes from irregular diamond crumbling to axisymmetric below folding when the thin shell are filled with foam. They tried out some theoretical studies to predict the average crushing load in both empty and filled tubes.

Reddy et al. [7] himself have studied the crushing behaviour of both empty and foam filled glass/epoxy and kelvar/epoxy tubes of round and rectangular cross sections. Tests were carried out in both quasi-static and dynamic condition and the results showed that the presence of foam increases the stability of the tube and increases its energy absorbing capability. Because of the complexities of crushing behaviour, much of the earlier studies were mainly experimental. Not much research or studies are available on the modeling of their deformation behaviour and predictions of the average crushing load, which is the main parameter in designing structures for crash-worthiness applications.

Robertson et al. [8], however, presented a simplified model to predict the average crushing stress of composite rods by considering various factors that influence their energy absorption. His model showed that the energy absorption properties of unidirectional fibre composite rods specimens were dependent on the fibre volume fraction and properties of the fibres and matrix, such as the fibre diameter, the matrix compressive strength and the bonding between the fibres and

matrix. The volume specific energy absorption was found to increase with fibre content, fibre diameter, matrix yield strength and crush rate.

Hull [9] summarized that the crush geometry and force-displacement response was interrelated and that the wide range of materials and testing variables that affected the crushing behaviour can be accounted for on this basis. The fracture mode of composite tubes made from brittle fibres and resins occurs by fragmentation or splaying, singly or in combination. These two different modes of fracture involved two completely different types of mechanisms. By changing the fibre distribution it was possible to change the micromechanisms of crush and hence control the load bearing capacity of the tubes during progressive crushing. For some fibre arrangement, the crushing speed had relatively little effect on the crushing behaviour and no change in crushing mode was observed. However, for some fibre arrangements, a small change in the crushing speed can caused a significant change in the crushing mode. Variables such as geometry and dimension can also affect the crush mode. It had been reported that for a same material with different values of Diameter (D), thickness (t) and D/t ratio, the different in the specific crushing stress was very significant.

Gupta and Velmurugan [10] studied the variation of the tube crush zone length (length crushed in a single cycle) with variation in its D/t ratio. Analysis was carried out to find the average crush stress for both empty and foam filled FRP tubes of different ratios under axial compression. The expressions are obtained by considering various energy terms involved in the crushing process. The average crushing stress obtained by the derived expressions are compared with

experimental results and results show that increase in D/t ratio increases the average crushing stress and the same was observed in the experimental values.

Hamada et al. [11] carried out compression tests to determine the effects of glass surface treatment on the crushing behaviour. The materials used were glass cloth/epoxy composite tubes with different glass/matrix surface treatment. Two kinds of surface treatment were used: acryl silane and amino silane coupling agents. The fracture mode of amino silane treated tubes was by splaying, whereas in the acryl treated tubes the fragmentation mode of crushing was observed. The axial crushing performance of the amino treated tubes is approximately 25 percent greater than the acrly treated ones.

Hull [9, 12] has demonstrated that a unifying theme is the influence of these many factors on the crush zone morphology, which, in turn, controls the ability of the crushing element to bear the load during crushing. The specific energy absorption, E_S, is defined as:

$$E_S = \sigma_{mean} K/\rho$$

Where σ_{mean} is the mean crush stress, ρ is the density and K is the efficiency factor relating to the way that crush debris is dispersed. Experiments have been carried out on the influence of fibre architecture and matrix properties on energy absorption in the carbon fibre/polymer-matrix composite tubes. The materials used were carbon/epoxy and carbon/PEEK composite tubes. The most remarkable feature of these results is the very high specific energy absorption (180 KJ Kg^{-1}) obtained in the 0° carbon/PEEK tubes. In contrast, the 0°

carbon/epoxy tubes failed at low loads with extensive cracking parallel to the fibres. The mode 1 fracture toughness (G_{Ic}) obtained for the carbon/PEEK was in the range 1560-2400 J m^{-2} and 120-180 J m^{-2} for the carbon/epoxy, using DCB (double cantilever bean) method. The compressive strength obtained on the 0˚ tubes show that, provided buckling is avoided, very high values (530 MPa for carbon/PEEK and more than 490 MPa for carbon/epoxy) can be achieved.

Hamada et al. [13] carried out further studies on the carbon fibre/PEEK to identify the factors, which contribute to the superior energy absorption performance of these tubes. The carbon fibre/PEEK tubes used in this study were the APC-2/AS4 with a volume fraction of 0.61. During axial compression loading of carbon/PEEK tubes, three steps sequentially take place prior to the establishment of a stable crush zone. First, the tube wall fractured and was followed by the longitudinal cracking of the tube wall. Lastly, longitudinal cracks cease to grow and the tube wall splays into internal and external fronds. These longitudinal cracks were observed to be ≈ 0.5 mm long, for carbon/PEEK, as compared to the 8 mm long cracks reported for carbon/epoxy tubes. During the steady-state progressive crushing, there were two main fracture processes, i.e., splitting of fronds into thin beams and fracture of fibres. It was found that the superior performance of the carbon/PEEK tubes is attributed to the higher fracture toughness of the composite materials, splitting of strands and the large number of fibre of fractures.

Dubey and Vizzini [14] compared the energy absorption of composite plates and tubes. All plate and tube specimens were manufactured from AS4/3501-6

graphite/epoxy with the same lay-up and thickness, thus providing a common laminate for comparison. Results indicated that specimen geometry affects specimen stability and therefore the failure modes exhibited by the specimen during crushing. Similar failure modes were observed in the tube and flat-plate specimens with the flat plates absorbing 12 percent less energy per unit mass. These can be attributed to the difference in the effective D/t ratio.

The influence of stacking sequence, trigger mechanism and thickness on energy absorption was investigated by Lavoie and Kellas [15]. Three materials systems were used by them: APC-2 (graphite/thermoplastic), AS-4/3502 (graphite/epoxy) and a hybrid AS-4/Kelvar-49/3502 (graphite/epoxy). The energy absorption of the composite plates investigated was strongly related to the crush mode. Farley [1,16] defines four crush modes: transverse shearing, brittle fracturing, lamina bending and local buckling. The crushing mode of a laminated composite plate was shown to depend on constituent materials and stacking sequence [17]. For the APC-2 plates the transverse shearing crushing mode was observed while the ply-level scaled APC-2 had a lamina-bending mode. This is why the energy absorption of ply-level scaled plates was only half of the sub-laminate level scaled plates. For the Graphite/Epoxy plates, delamination and lamina-bending were the main mode of crushing. The Graphite-kelvar/Epoxy plates had lower energy absorption than the Graphite/Epoxy plates because the Kelvar fibres are weaker in compression and much less stiff than graphite fibres, hence the lower absorption capacity.

The specific energy absorption capability of knitted fabric composite increased with the fibre content [18]. Tubes with inlay fibres displayed higher specific energy than tubes with hoop inlay fibres. A maximum 85 KJ Kg^{-1} specific energy was absorded by tubes with axial inlay fibres containing 22.5 vol% of fibres. This may be compared with the 120 KJ Kg^{-1} absorbed by the carbon/epoxy tubes with $[0\pm15]_4$ fibre lay-up containing 45 vol% of fibres [21]. It is possible to achieve fibre volume fractions as high as 40% in knitted fabric composites [22]. Karbhari [20] showed that hybrid glass/carbon triaxial braid, with 6 thousand carbon fibres, yielded a specific energy absorption of 64.21 KJ Kg^{-1} on the average (70 KJ Kg^{-1} at the maximum). The glass/Kelvar biaxial hybrid, however, had a mean SEA (specific energy absorption) of only 30.7 KJ Kg^{-1}. Table 2.1 summarizes some of SEA values from various papers and technical journals:

Table 2.1: Summary of Specific Energy Absorption (SEA) Values

Materials Systems	SEA (KJ Kg^{-1})	References
Carbon/PEEK (with t/D ratio between 0.06 – 0.10)	205	23
Glass/Carbon Triaxial	64.21	20
Glass/Kelvar Biaxial	30.7	20
Knitted Fabric (axial inlay, 22 vol%)	85	18
Glass Fibre Reinforced Plastic (GrFRP) with 0/90 lay-up	40	24
Graphite Fibre Reinforced Plastic (GFRP) with 0/90 lay-up	60	24
T650-35/F584 Graphite/Epoxy $[45_2/0_2/45]_s$	98.1	25
T650-35/F584 Graphite/Epoxy $[45_2/0/45]_s$	94.9	25
T650-35/F584 Graphite/Epoxy $[45]_{10}$	91.1	25
Glass Cloth/Epoxy (acryl-silane treated)	53	11
Glass Cloth/Epoxy (amino-silane treated)	66.6	11
AS4/APC-2 Carbon/PEEK (lay-up ± 30º)	127	12
AS4/APC-2 Carbon/PEEK (lay-up 0º)	180	12
Q-112/HTA Carbon Fibre/Epoxy (lay-up ± 45º)	45	12
APC-2 (laminate type – ply-level)	89.4	15
AS-4/3502(laminate type – ply level)	49	15
AS-4-Kelvar/3502 (laminate type – ply level)	43.4	15
XAS/BSL914 Carbon/Epoxy (with hoop to axial fibre ratio of 1 : 3)	120	Grundy (See [9])

2.2 Strain Energy Release Rate and Interlaminar Fracture Toughness of Composite Materials [29]

Analysis of the strain energy rate of a given geometry and loading is vital for the prediction of delamination or interlaminar flaw growth. Wang [26] overviewed the fracture mechanics approach as applied to composite materials, using the strain energy release rate as a crack extension criterion. Wang et al. [26, 27, 28] calculated the strain energy release rate using the crack closure method and made prediction based on the critical strain energy release rate, which were obtained through experiments. They succeeded in predicting the onset of edge delamination in $(\pm 25/90_n)_s$ laminates.

O' Brien [29] derived a simple closed form equation for the strain energy rate, *G*, associated with edge delamination growth in unnotched laminates by using the laminated plate theory. Results of *G* using his equation were in good agreement with finite element analysis. His findings led to the use of the edge delamination test as a proposed standard test for fracture toughness.

The most commonly used test for interlaminar fracture toughness characterization in mode 1 is the DCB (double cantilever beam) test. Two basic configurations were used, the constant width and the tapered width.

Strain energy release rate obtained by the WTDCB (tapered width) is independent of crack length, *a*, the crack grows under a constant load [30]. Using the DCB, Ramkumar and Whitcomb [31] characterized the interlaminar fracture toughness of the T300/5208 composite laminates. Two lay-up configurations

were used and the G between the two lay-up was small (G_{Ic} = 102.6 J m^{-2} for the 0_{24} specimens and 100 J m^{-2} for the $(0_2/\pm45/0)_S$ specimens).

Hunston and Bascom [32, 33] showed that the fracture energy rate of an elastomer in a function of temperature and loading rate. They measured the G_{Ic} of the composite using the DCB test and found that no significant variations between -25º and 40º at cross head speeds from 0.0008 – 0.8 mms^{-1}. Table 2.2 summarizes some of the published data of G_{Ic} for different materials tested by various test methods:

Table 2.2: Values of Energy Release Rate (G_{Ic}) from published papers

Materials	Type of Test	G_{Ic} J m^{-2}	Reference	Remarks
T300/5208	DCB, 0_{24}	102.3	31	
T300/5208	DCB, $[0_2/\pm45/0]_s$	100	31	
T300/5208	DCB	87.5	34	
Gr/5280	WTDCB	88	35	
Gr/F-185	WTDCB	1884	35	
Gr/F-185	EDT, $[\pm30_S/90/90]_S$	2140	35	
AS1/3501-6	DCB	103	36	
T300/934	DCB	103	36	
AS4/3501-6	DCB	198	37	Loading rate at 0.0085 mm/s
AS4/3501-6	DCB	254	37	Loading rate at 8.47 mm/s
AS4/3501-6	DCB, 0_{24}	190	38	
CYCOM 982	DCB	680	38	
AS4/PEEK (APC-2)	DCB, 5.6mm thick	2890	38	

AS4/PEEK (APC-2)	DCB	1750	38	
AS1/3502	DCB	140	39	
XAS/PEEK (APC-1)	DCB	1408	39	
XAS/PEEK (APC-1)	EDT, $[+30_2/30_2/90_2]_S$	1408	39	
AS1/3502	DCB	155	40	
AS4/3502	DCB	225	40	
AS1/3502	DCB, 0_{24}	140	41	
AS4/3502	DCB, 0_{24}	160	41	
AS4/3502	DCB, 0_{24}	158	42	
T300/F-185	WTDCB	1880	43	
AS4/PEEK	DCB	1330	44	
AS1/3502/163	DCB	128.8	45	
AS1/3502/163 (Kelvar mat)	DCB	1855	45	
AS4/3502 (0.1 mm adhesive)	DCB	1140	46	
AS1/3502/AF163U	DCB	1280	47	

Chapter 3

Theories

3.1 Linear Elastics Fracture Mechanics (LEFM)

The elastics fracture mechanics deals with the prediction of fracture strength of relatively brittle materials. The linear elastic materials are assumed to be isotropic and contain pre-existing cracks. In the analysis of the problem in this project, the energy release rate approach of the linear elastics fracture mechanics was used.

The first successful analysis of the energy release rate method was that of Griffith in 1920. His reasoning was based on the hypothesis that the free energy of a cracked body and the applied force should not increase during crack extension. This hypothesis allows the estimation of the theoretical strength and also gives the correct relationship between fracture strength and defect size. The general equation of the Griffith's energy approach was given as [34]

$$\frac{d}{da}\left(F - U_a\right) \geq \frac{dU_\gamma}{da} \qquad \text{.....(3.1)}$$

In 1948, Irwin pointed out that the Griffith type energy balance must be between

(1) the stored strain energy and

(2) the surface energy plus the work done in plastic deformation

and Irwin defined a material property *G* as the total energy absorbed during cracking per unit increase in crack length and per unit thickness. This material property *G* is called the "crack driving force" or "energy release rate" [35].

Since the right hand side of Griffith's equation is the total energy absorbed during cracking and *G* as defined by Irwin is the total energy absorbed during cracking, therefore Griffith's equation can be re-written as

$$G = \frac{d}{da}(F - U_a) \qquad \text{.....(3.2)}$$

In this project, the crack between the piles were model as a double cantilever beam (DCB) specimen as shown below. For a DCB specimen the force *F* is equal *Pv* and U_a is equal to half of the force. Figure 2.1 shows a typical DCB specimen configuration.

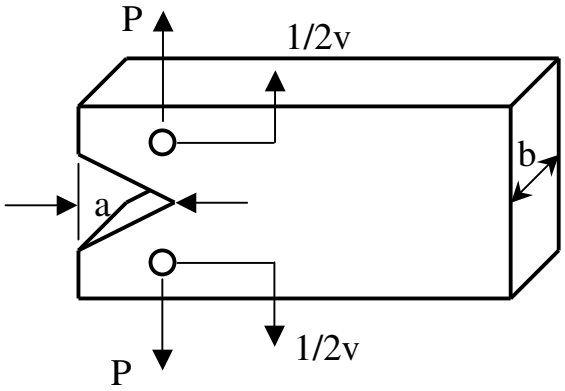

Figure 2.1 : A typical DCB specimen configuration

Therefore Equation (3.2) can be written as

$$G = \frac{d}{da}\left(F - U_a\right) = \frac{1}{b}\left(P\frac{dv}{da} - \frac{dU_a}{da}\right)$$

$$= \frac{1}{b}\left(P\frac{dv}{da} - \frac{dPv}{2da}\right) \qquad \text{.....(3.3)}$$

By introducing the compliance of the body, *C*, which is the inverse of the stiffness, i.e.

$$C = \frac{v}{P}$$

the above equation (3.3) becomes

$$G = \frac{P^2}{2b}\left(\frac{dC}{da}\right) \qquad \text{.....(3.4)}$$

for a Mode I, double cantilever beam (DCB)

$$\frac{dC}{da} = \frac{24a^2}{Ebh^3} \qquad \text{.....(3.5)}$$

therefore the energy release rate *G* is equal (substituting 3.5 into 3.4)

$$G = \frac{12P^2a^2}{Eb^2h^3} \qquad \text{.....(3.6)}$$

3.1.1 Relationship of *G* and the Stress Intensity Factor K_I

For a plane stress condition,

$$\frac{dU_a}{da} = G = \frac{\pi\sigma^2 a}{E} \qquad \text{……(3.7)}$$

and the stress intensity factor K_I is equal to $\sigma\sqrt{\pi}a$ and substituting into the above equation we obtain

$$G = \frac{K_1^2}{E} \qquad \Rightarrow K_I = \sqrt{GE} \qquad \text{……(3.8)}$$

The above equation shows that under LEFM condition, the prediction for crack growth and fracture is the same for both the energy balance and the elastic stress field approach.

3.2 Buckling Theory

For the simplicity of analysis, the fiber strands subjected to the axial load were modelled as miniature columns. Using the buckling of column of strength of materials studies, one can determine the critical load acting on the fiber strand.

The critical load can be obtained by considering the behaviour of an ideal column, which assumed initially to be perfectly straight and compressed by a centrally applied load. The column is assumed to be perfectly elastic and when a load P is applied, will remain straight and undergoes only axial deflection. Therefore the moment at any cross section is given as

$$M = -P(\delta - y) \qquad \text{…….(3.9)}$$

and the differential equation is

$$EI\frac{d^2y}{dx^2} = -P(\delta - y) \qquad \text{…….(3.10)}$$

By integration, the solution of the above differential equation is

$$y = A\cos kx + B\sin kx + \delta \qquad \text{……(3.11)}$$

Applying the boundary conditions, one can obtain the applied load expression as follows

$$(2n-1)\frac{\pi}{2} = l\sqrt{\frac{P}{EI}} \qquad \text{……(3.12)}$$

Since for $n > 1$ has no physical significance, therefore the smallest value of P will be when $n = 1$

$$P_{cr} = \frac{\pi^2 EI}{4l^2} \qquad \text{.....(3.13)}$$

The critical load P_{cr} is also know as the Euler load and is defined as the axial force which is sufficient to keep the bar in a slightly bent form.

3.3 Some limitation on the theories used

Since no material can withstand a stress, which is infinite in magnitude, the material in the vicinity of the crack tip is deformed in the plastic manner. As a result, the linear elastic fracture mechanics approach is valid for low nominal stress wherein the plastic zones are small relative to crack size and specimen boundaries and are totally confined in the elastic regions.

The stress intensity factor provides a reasonably good approximation for stresses inside the unstable fracture region. But the expression for stress intensity factor is difference for loading conditions and modes of failure and the expression can be quite difficult to solve for same loading conditions.

Chapter 4

Formulation of Equation

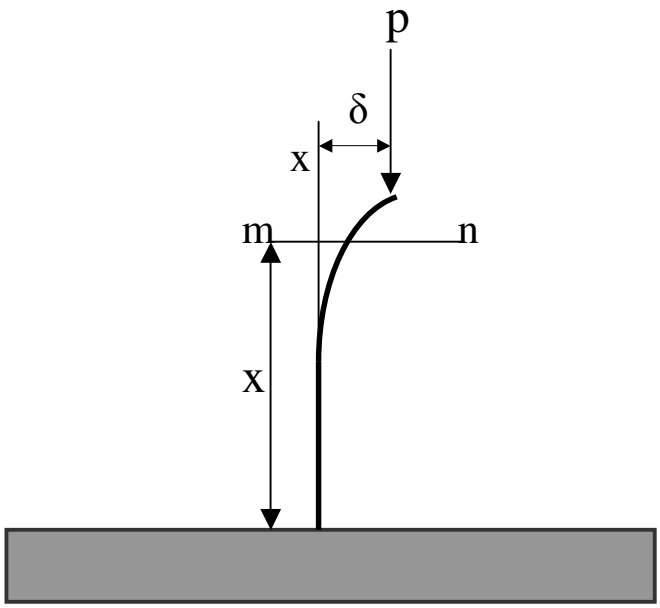

Figure 4.1 : Diagram for formulation of equation

From figure 4.1 the bending moment at any cross section *mn* is

$$M = -P(\delta - y) \qquad \text{.....(3.9)}$$

and the differential equation is

$$EI\frac{d^2y}{d^2x} = P(\delta - y) \qquad \text{.....(3.10)}$$

where *I* is the moment of inertia for buckling at the *xy* plane. Since

$$k^2 = \frac{P}{EI} \qquad \text{……..(4.1)}$$

one can write Equation (3.10) in the form of

$$\frac{d^2y}{d^2x} + k^2 y = k^2 \delta \qquad \text{……..(4.2)}$$

since this is a non-homogenous 2nd order ordinary differential equation, the general solution of this equation is :

$$y = A\cos kx + B\sin kx + \delta \qquad \text{……..(3.11)}$$

To find the constants *A* and *B*, the two conditions at the fixed end of the bar were used,

$$y = \frac{dy}{dx} = 0\,, \qquad \text{at } x = 0$$

These two conditions are fulfilled if

$$A = -\delta\,, \qquad B = 0$$

and then

$$y = \delta(1 - \cos kx) \qquad \text{…….(4.3)}$$

The condition at the upper end of the bar requires that

$$y = \delta \qquad \text{at } x = 1$$

which is satisfied if

$$\delta \cos kl = 0$$

If $\delta = 0$, there is no deflection and hence no buckling, if $\cos kl = 0$, then we must have the relation

$$kl = (2n-1)\frac{\pi}{2} \qquad \text{.....(4.4)}$$

For the smallest P, n must be equal to 1, therefore

$$kl = l\sqrt{\frac{P}{EI}} = \frac{\pi}{2} \qquad \text{.....(4.5)}$$

from which

$$P_{cr} = \frac{\pi^2 EI}{4l^2} \qquad \text{.....(3.13)}$$

For a Mode I DCB specimen (as shown in figure 4.2),

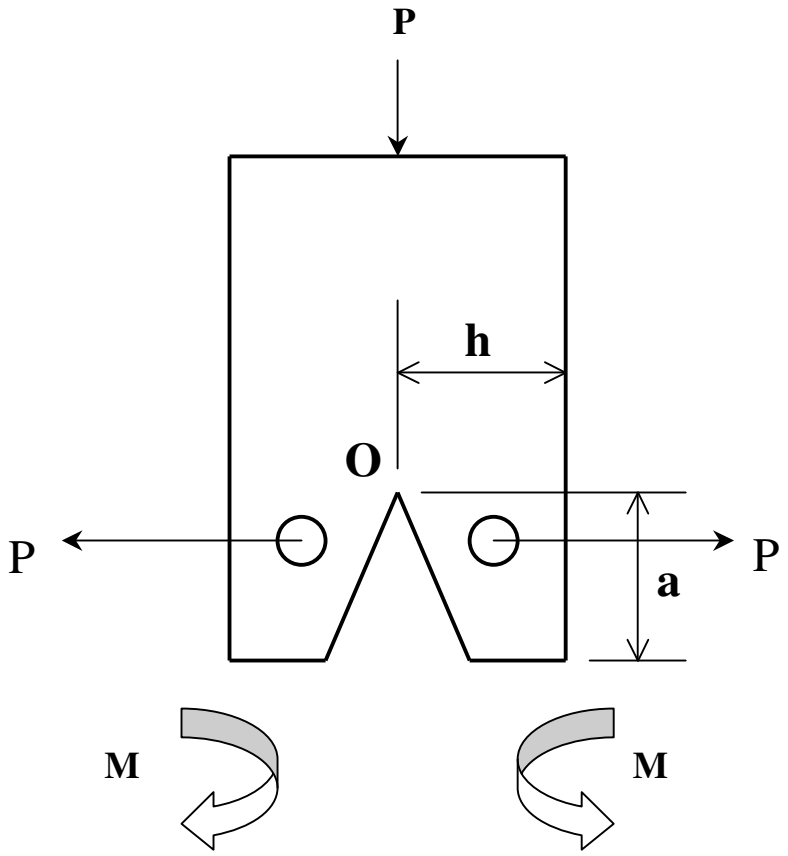

Figure 4.2 : Mode I DCB Specimen

the energy release rate is given as

$$G = \frac{12P^2a^2}{Eb^2h^3} \qquad \text{……..(4.6)}$$

where *Pa* is the moment about O (Figure 4.2).

In order to compute the moment about O, consider the free body diagram in figure 4.3

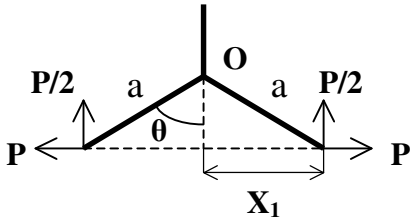

Figure 4.3 : Free Body Diagram

The moment about O due to the force *P/2* is

$$M_1 = \frac{p}{2} a \sin\theta \qquad \text{.....(4.7)}$$

The moment due to buckling on one arm of the specimen is

$$M_2 = -Px_1 \qquad \text{where } x_1 = a\cos\theta, \quad \text{and } P = P_{cr}$$

which gave

$$M_2 = -\frac{\pi^2 EI}{4l^2} a\cos\theta \qquad \text{.....(4.8)}$$

Therefore total moment about O is,

$$M_T = M_1 + M_2$$

$$= \frac{P}{2} a \sin\theta - \frac{\pi^2 EI}{4l^2} a \cos\theta \quad \text{.....(4.9)}$$

For Mode I energy release rate and re-arranging Equation (b), we obtain

$$Pa = \sqrt{\frac{GEb^2h^3}{12}} \quad \text{.....(4.10)}$$

Since *Pa* is the moment about O, therefore

$$Pa = M_T = \frac{P}{2} a \sin\theta - \frac{\pi^2 EI}{4l^2} a \cos\theta \text{ ....(4.11)}$$

Substituting into Equation (4.10)

$$\frac{p}{2} a \sin\theta - \frac{\pi^2 EI}{4l^2} a \cos\theta = \sqrt{\frac{GEb^2h^3}{12}} \text{ ....(4.12)}$$

divide both side by *a sin θ*

$$\frac{p}{2} - \frac{\pi^2 EI}{4l^2} \sec\theta = \frac{1}{a \sin\theta} \sqrt{\frac{GEb^2h^3}{12}} \text{ .....(4.13)}$$

Re-arranging the equation to obtain the force *P*

$$P = \frac{2}{a\sin\theta}\sqrt{\frac{GEb^2h^3}{12}} + \frac{\pi^2 EI}{2l^2}\sec\theta \qquad \text{.....(4.14)}$$

The moment of inertia I is given as

$$I = \frac{bh^3}{12}$$

Substituting into Equation (4.14), one obtain

$$P = \frac{2}{a\sin\theta}\sqrt{\frac{GEb^2h^3}{12}} + \frac{\pi^2 Ebh^3}{24l^2}\sec\theta \qquad \text{.....(4.15)}$$

The mean crushing stress, σ_c, is given as

$$\sigma_c = \frac{P}{A} \qquad \text{.....(4.16)}$$

Therefore Equation(4.15) becomes

$$\frac{P}{A} = \sigma_c = \frac{2}{a\sin\theta A}\sqrt{\frac{GEb^2h^3}{12}} + \frac{\pi^2 Ebh^3}{24l^2 A}\sec\theta \text{.....(4.17)}$$

where *A* is the area of one limb of the specimen and is equal to *bh.*

Substituting *bh* into the above equation and re-arranging the terms, one obtains

$$\sigma_c = \frac{1}{a\sin\theta}\sqrt{\frac{GEh}{3}} + \frac{\pi^2 Eh^2}{24l^2}\sec\theta \qquad \text{.....(4.18)}$$

Since the above derivation is for one limb only, and for the whole specimen, the mean crushing stress is

$$\sigma_c = \frac{2}{a\sin\theta}\sqrt{\frac{GEh}{3}} + \frac{\pi^2 Eh^2}{12l^2}\sec\theta \qquad \text{.....(4.19)}$$

We can also re-arrange Equation (3-3) to obtain the energy release rate *G*

$$G = \frac{3(a\sin\theta)^2}{Eh}\left(\frac{\sigma_c}{2} - \frac{\pi^2 Eh^2\sec\theta}{24l^2}\right)^2 \qquad \text{.....(4.20)}$$

Chapter 5

Results and Discussions

For the convenience of comparison and calculation, the following assumption were made,

a. A crack angle of 30º was used for all comparison.

b. A crack length of 5mm was used on all specimens.

c. The energy release rate of all the specimens was on values obtained by the double cantilever beam (DCB) method.

The values used for all calculations were obtained from Hamada et al. [11], [12] and Hamada et al. [61]. Table 5.1 summarizes the data used for calculations,

Table 5.1: Data used for calculations

S/No	Materials used	E (GPa)	ρ (kg/m^3)	*l* (mm)	h (mm)	G (N/m)
1	C/PEEK (0˚)	131	1700	55	1.25	1560
2	C/PEEK (30˚)	65	1700	55	1.25	1560
3	C/EPOXY (45˚)	66	1500	55	1.25	120
4	GL/CLOTH-EPOXY #1	21.4	2020	55	1.25	1207
5	GL/CLOTH-EPOXY #2	20.9	2020	55	1.25	1196
6	GL/CLOTH-EPOXY #3	21.4	2020	55	1.25	979
7	GL/CLOTH-EPOXY #4	20	2020	55	1.25	1038
8	C/PEEK (B16)	134	1600	55	1.10	1750
9	C/PEEK (N16)	134	1600	55	1.045	1750
10	C/PEEK (N20)	134	1600	55	1.33	1750
11	C/PEEK (L116)	134	1600	55	1.07	1750

5.1 Calculation of σ_c using Equation (4.19)

Equation (4.19) was derived using LEFM (Linear Elastic Fracture Mechanics) and simple beam theory.

$$\sigma_c = \frac{2}{a\sin\theta}\sqrt{\frac{GEh}{3}} + \frac{\pi^2 Eh^2}{12l^2}\sec\theta \qquad \text{.....(4.19)}$$

The calculated values of Equation (4.19) were compared with values obtained from technical papers and research journals. Table 5.2 shows the comparison of both values.

Table 5.2 : Comparison of Crushing Stresses

S/No	Materials Used	σ_c (from Refs) x 10^6	σ_c (using Eqn 3-3) x 10^6	Percentage Error (%)
1	C/PEEK (0°)	283	297	4.95%
2	C/PEEK (30°)	190	196	3.16%
3	C/EPOXY (45°)	79	78	1.27%
4	GL/CLOTH-EPOXY #1	110	93	15.45%
5	GL/CLOTH-EPOXY #2	106	92	13.20%
6	GL/CLOTH-EPOXY #3	91	85	6.59%
7	GL/CLOTH-EPOXY #4	90	84	6.67%
8	C/PEEK (B16)	327	285	12.84%
9	C/PEEK (N16)	334	274	17.96%
10	C/PEEK (N20)	356	332	6.74%
11	C/PEEK (L116)	309	279	9.71%

Using Equation (4.19), one can plot the graphs for the following conditions

a) crushing stresses **versus** the crack length (a), plotted in figure 5.1

b) crushing stresses **versus** the thickness (h), plotted in figure 5.2

c) crushing stresses **versus** the cracking opening (θ), plotted in figure 5.3

All the plotted figures are shown in the following pages. A typical mean crush load-thickness figure 5.4 from reference Kim et al. [68] is attached as a comparison with figure 5.2.

5.2 Calculating Energy Release Rate (*G*) using Equation (4.20)

By re-arranging Equation (4.19), we obtain the energy release rate (G) in term of the stress (σ_c), and the thickness (h). The equation is shown below,

$$G = \frac{3(a\sin\theta)^2}{Eh}\left(\frac{\sigma_c}{2} - \frac{\pi^2 Eh^2 \sec\theta}{24l^2}\right)^2 \qquad \text{.....(4.20)}$$

Calculated values of G using Equation (4.20) are compared with values obtained from technical or research papers. Table 5.3 shows the comparison of these two values.

Table 5.3 : Comparison of *G* values

S/No	Materials Used	G (from Refs)	G (using Eqn 3-4)	Percentage Error (%)
1	C/PEEK (0°)	1560	1551	0.58%
2	C/PEEK (30°)	1560	1554	0.38%
3	C/EPOXY (45°)	120	118	1.67%
4	GL/CLOTH-EPOXY #1	1207	1193	1.16%
5	GL/CLOTH-EPOXY #2	1196	1485	24.16%
6	GL/CLOTH-EPOXY #3	979	973	0.61%
7	GL/CLOTH-EPOXY #4	1038	1032	0.59%
8	C/PEEK (B16)	1750	1746	0.23%
9	C/PEEK (N16)	1750	1744	0.34%
10	C/PEEK (N20)	1750	1750	0.00%
11	C/PEEK (L116)	1750	1746	0.23%

5.3 Discussions

Comparison between the values calculated using Equation (4.19) and Equation (4.20) and values taken from research and technical papers were presented in Tables 5.1 and 5.2. Comparisons were done on seven types of carbon fibres composites and 4 types of glass-cloth/epoxy composites. In these analysis, the derived model has been fixed with the following parameters :

a) a length of 55mm

b) a crack opening angle of 30°

c) a crack length of 5mm for Equation (4.19)

For the crushing stress calculation, the comparison between the calculated results and experimental values seems reasonable. In the carbon fibre specimens, the largest percentage error was 17.96% and the least was 1.27%. Overall, the average error was about 8.09%.

For the glass-cloth/epoxy composites, the largest percentage error was 15.45% and the least was 6.59%. And average error of 10.48% was recorded for the glass-cloth/epoxy.

The energy release rate calculations were based on mean stress values obtained from experiments carried out by established sources. The average error obtained was about 0.49% and 6.63% for the carbon fibre specimens and glass-cloth/epoxy composites respectively; this error is even smaller compared to the crushing stress calculations.

Figure 5.1 shows the stress-crack length curves for the various composites specimen versus the experimental values obtained from Hamada et al. [66].

From the figure 5.1, one can observe that carbon fibre specimens with a lower angle of fibre orientation agree quite well with the experimental data. As for the carbon fibre specimen of 45°, the error was quite substantial as compared with the experimental data. One likely cause of this large error is the effect of transverse ply cracking of the 45° specimen, which leads to localized fibre breakage.

Figure 5.2 shows the plot of crushing stress against the thickness, *h*. From the graph one can observe that the crushing stress or load increase as the thickness increase, this theoretical observation show a good agreement with experimental observation [67] which is shown in figure 5.4.

The term $\sqrt{GE}$ in Equation (4.19) is the stress intensity factor of a material. The stress intensity factor of any material depends on the loading conditions and the mode of failure, i.e. Mode I, Mode II or mixed mode. Because of the nature of composite materials, the stress intensity factor can be quite difficult to obtain. Therefore the validity of stress intensity factors in composite materials is still an uncertainty and this may be the cause of the errors presented in the calculations.

Chapter 6

Conclusion and Recommendations

In this project, Euler's buckling equation was used to derive the critical load (P_{Cr}) of the composite material. After obtaining the critical load, simple mechanics was used to find the moment acting on one limb of the model. Linear elastic fracture mechanics (LEFM) was used to derive the Mode I energy release rate (*G*). And equation (4.19) and (4.20) are derived based on these two engineering concepts.

Certain assumptions were made when deriving the equation:

1) Linear elastics properties were assumed.

2) Thermal expansions between the piles were not considered.

3) Other modes of energy release rates were assumed to be negligible.

The calculated stresses and energy release rates were compared with experimental values obtained from research or technical papers. The results obtained can be summarized below:

- Results obtained from Equation (4.19) and (4.20) agreed quite well with experimental values.

- The plotted curves of Equation (4.19) in figure 5.2 agreed with established plot of the same nature.

- The Stress Intensity Factor, K_1 term in Equation (4.19) played an apart in the error obtained, because the validity of K_1 in composite is quite difficult to obtain due to the complex nature of the damage mechanisms.

The derived equation can predict or provide a reasonable stress prediction for most composite systems. The variables in the derived equation can be directly measured by experiments or can be obtained from handbooks or journals.

The mode of failure of the derived equation was based only on Mode I failure. It was therefore recommended that any future works or analysis on this project should include the other two modes of failures, i.e. Mode II and Mode III or the mixed mode.

Another area of interest for future development is the stress intensity factor (K_1).

The stress intensity factor for Mode I plane stress is given as

$$K = \sqrt{GE} \qquad \text{……..(3.8)}$$

and this term is present in Equation (4.19).

Since there is no standard stress intensity factor solution, it might therefore be interesting to observe what might happen if different solutions of stress intensity factors were used.

Implementation of a program using software such as Mathlab for easy calculation and comparison of data by other user can also be consider for future works.

References

1. Farley G.L and Jones R.M., **"The Effect of Crushing Speed on the Energy Absorption Capability of Composite Tubes."**, *Journal of Composite Materials*, 1991, V26, pg 1314-1329.

2. Farley G.L and Jones R.M., **"Prediction of the Energy Absorption Capability of Composite Tubes"**, *Journal of Composite Materials*, 1992, V26, pg388-404.

3. Thornton P.H., **"Energy Absorption in Composite Structure."**, *Journal of Composite Materials*, 1979 V13, pg 247-263.

4. Thornton P.H., and Edwards P.J., **"Energy Absorption in Composite Tubes."**, *Journal of Composite Materials*, 1982, V16, pg 521-545.

5. Fairfull A.H. and Hull D., **"Energy Absorption of Polymer Matrix Composite Structure: Frictional Effects."**, *Structural Failure*, 1989, pg, pg 521-545.

6. Reddy T.Y. and Wall R.J., **"Axial Compression of Foam Filled Thin Walled Circular Tubes."**, *International Journal of Impact Engineering*, 1988, V7, pg 151-166.

7. Lampinen B.E. and Jeryan R.A., **"Effectiveness of Polyurethane Foam in the Energy Absorbing Structures"**, *Society of Automotive Engineers, Transaction*, 82094, 1983, pg 2059-2076

8. Tao W.H., Robertson R.E. and Thornton P.H**., "Effect of Materials Properties and Crush Conditions on the Crush Energy Absorption of Fibre Composite Rods."**, *Composites Science and Technology*, 1991, V47, pg 405-418.

9. Hull D., **"A Unified Approach to Progressive Crushing of Fibre-Reinforced Composite Tubes."**, *Composites Science and Technology*, 1991, V40, pg 377-421.

10. Gupta N.K., Velmurugan R. and Gupta S.K., **"An Analysis of Axial Crushing of Composite Tubes."**, *Journal of Composite Materials*, 1997, V31, pg 1262-1286.

11. Hamada H., Coppola J.C., And Hull D., **"Effect of Surface Treatment on Crushing Behaviour of Glass Cloth/Epoxy Composite Tubes."**, *Composites*, 1992, V23, pg 93-99.

12. Hamada H., Coppola J.C., Hull D., Maekawa Z. and Sato H., **"Comparison of Energy Absorption of Carbon/Epoxy and Carbon/PEEK Composite Tubes."**, Composites, 1992, V23, pg 245-252.

13. Hamada H., Ramakrishna S., Satoh H., "**Crushing Mechanism of Carbon Fibre/PEEK Composite Tubes."**, *Composites*, 1995, V26, pg 749-755.

14. Dubey D.D. and Vizzini A.J., "**Energy Absorption of Composite Plates and Tubes."**, *Journal of Composite Materials*, 1998 V32, pg 158-176.

15. Lavoie J.A. and Kellas S., **"Dynamic Crush Tests of Energy Absorbing Laminated Composite Plates."**, *Composites Part A*, 1996, V27A, pg 467-475.

16. Farley G.L. and Jones R.M., **"Energy Absorption Capability of Composite Tubes and Beams"**, *NASA TM 101634*, 1989.

17. Lavoie J.A., Morton J. and Jackson K., **"An Evaluation of the Energy Absorbing Laminated Composite Plates."**, *Proceedings of the Institute of Mechanical Engineers*, 1995, V209, pg 185-194.

18. Ramakrishna S. and Hull D., **"Energy Absorption Capability of Epoxy Composite Tubes with Knitted Carbon Fibre Fabric Reinforcement."**, *Composites Science and Technology*, 1993, V49, pg 349-356.

19. Karbhari V.M., Falzon P.J. and Herzberg I., **"Energy Absorption Characteristics of Hybrid Braided Composite Tubes."**, *Journal of Composite Materials*, 1999, V33, pg 1164-1185.

20. Karbhari V.M., Falzon P.J. and Herzberg I., **"Energy Absorption Characteristics of Stitched Composite Sandwich Panels."**, *Journal of Composite Materials*, 1999, V33, pg 712-727.

21. Farley G.L., **"Energy Absorption Composite Materials and Structures."**, *Proceedings of the 43rd American Helicopter Society Annual Forum*, 1987, pg 613-627.

22. Williams D., **"New Knitting Methods Offer Continuous Structures."**, *Advanced Composites Engineering*, 1987, June, pg 12-13.

23. Hamada H., and Ramakrishna S., **"Scaling Effects in the Energy Absorption of Carbon Fibre/PEEK Composite Tubes."**, *Composites Science and Technology*, 1995, V55, pg 211-221.

24. Thornton P.H., Harwood J.J and Beardmore P., **"Fibre Reinforced Plastic Composite for Energy Absorption Purposes."**, *Composites Science and Technology*, 1985, V24, pg 275-297.

25. Bolukbasi A.O. and Laananen D.H., **"Analytical and Experimental Studies of Crushing Behaviour in Composite Laminates."**, *Journal of Composite Materials*, 1995, V29, pg 1117-1139.

26. Wang A.S.D., **"Fracture Mechanics of Sublaminate Cracks in Composite Laminates."**, *Composite Technology Review*, 1984, V6, pg45-62.

27. Crossman F. and Wang A.S.D., **"The Dependence of Transverse Cracking and Delamination on Ply Thickness in Graphite/Epoxy Laminates."**, *ASTM STP 775*

28. Law G.E., **"A Mixed Mode Fracture Analysis of $(\pm 25/90_n)_s$ Graphite/Epoxy Composite Laminates."**, *ASTM STP 836*, 1984, pg 143-160.

29. O'Brien T.K., **"Characterization of Delamination Onset and Growth in a Composite Laminate."**, *ASTM STP 775*, 1982, pg 140-167.

30. Sela N. and Ishai O., **"Interlaminar Fracture Toughness and Toughening of Laminated Composite Materials: A Review."**, *Composite*, 1989, V20, pg 423-435.

31. Ramkumar R.L and Whitcomb J.D., **"Characterization of Mode 1 and Mixed Mode Delamination Growth in T300/5208 Graphite/Epoxy."**, *ASTM STP 876*, 1985, pg 315-335.

32. Hunston D.L., **"Characterization of Interlaminar Crack Growth in Composites with the DCB specimen."**, *Tough Composite Materials, Recent Developments*, NASA, 1985, pg 2-13.

33. Hunston D.L. and Bascom W.D., **"Effects of Lay-up, Temperature and Loading Rate in DCB Tests of Interlaminar Crack Growth."**, *Composites Technology Review*, 1983, V5, pg 118-119.

34. Wilkins D.J., Eisenmann J.R., Chamin R.A., Margolis W.S. and Benson R.A., **"Characterizing Delamination Growth in Graphite/Epoxy."**, *ASTM STP 775*, 1982, pg 168-183.

35. O'Brien T.K., Johnston N.J., Morris D.H. and Simonds R.A., **"A Simple Test for the Interlaminar Fracture Toughness of Composite."**, *SAMPLE Journal*, 1982, pg 8-15.

36. Garg A. and Ishai O., **"Hygrothermal Influence on Delamination Behaviour of Graphite/Epoxy Laminates."**, *Engineering Fracture Mechanics*, 1985, V22, pg413-427.

37. Aliyu A.A. and Danial I.M., **"Effects of Strain Rate on Delamination Fracture Toughness of Graphite/Epoxy."**, *ASTM STP 876*, 1985, pg 336-348.

38. Gillespie J.W., Carlsson L.A. and Smily A.J., **"Rate Dependent Mode 1 Interlaminar Crack Growth Mechanisms in Graphite/Epoxy and Graphite/PEEK."**, *Composites Science and Technology* , 1987, V28, pg 1-15.

39. Browning D.E., **"Composite Materials Characterization and Development at AFWAL."**, pg 28-53.

40. Bradley W.L. and Cohen R.N., **"Matrix Deformation and Fracture in Graphite Reinforced Epoxies."**, *ASTM STP 876*, 1985, pg 389-410.

41. Whitney J.M., Browning C.E. and Hoogsteden W.A., **"A DCB Test for Characterizing Mode 1 Delamination of Composite Materials."**, *Journal of Reinforced Plastics and Composites*, 1982, V1, pg 297-313.

42. Whitney J.M. and Knight M.K., **"A Modified Free Edge Delamination Specimen."**, *Delamination and Debonding of Materials*, *ASTM STP 876*, 1985, pg 314.

43. Daniel I.M., Shareef I. and Aliyu A.A., **"Rate Effects on Delamination Fracture Toughness of a Toughened Graphite/Epoxy."**, *ASTM Symposium on Toughened Composites,* March 1985.

44. Russell A.J. and Street K.N., **"Moisture and Temperature Effects on the Mixed Mode Delamination Fracture of Unidirectional Graphite/Epoxy."**, *ASTM STP 876*, 1985, pg 349-370.

45. Browning C.E. and Schwartz H.S., **"Delamination Resistant Composite Concepts."**, *ASTM STP 893*, 1986, pg 256-265.

46. Sela N., Ishai O. and Banks-Sills L., **"The Effects of Adhesive Thickness on Interlaminar Fracture Toughness of Interleaved CFRP specimens."**, *Composites*, 1989, V20, pg 257-264.

47. Whitney J.M., Browning C.E., **"Materials Characterization for Matrix Dominated Failure Modes."**, *ASTM STP 836*, 1984, pg 104-124.

48. Wolff C., Bastid P. and Bunsell A.R., "**Relation of Energy Absorption of Composite Structures To Material Strength.",** *Composites Engineering*, 1994, V4, pg 195-218.

49. Timoshenko and Gere, "Theory of Elastic Stability",1961.

50. Chiu C.H., Lu C.K. and Wu C.M., "**Crushing Characteristics of 3-D Braided Composite Square Tubes.**", *Journal of Composite Materials*,1997, V31, pg 2309-2327.

51. Harris B., Dorey S.E. and Cooke R.G., "**Strength and Toughness of Fibre Composites.**", *Composites Science and Technology*, 1988, V31, pg121-141.

52. Mallick P.K. "**Composite Engineering Handbook.**"

53. Fairfull A.H., & Hull D. "**Effects of specimen dimensions on the specific energy absorption of fibre composite tubes.**" *6th ECCM and ICCM*, Vol 3, pg 36-45.

54. Hull D., "**The crush performance of composite structures.**" *Composite Structure,* Vol 2, pg 32-44.

55. Kirsch P.A. & Jahnle H.A., "**Energy absorption of glass-polyester structures.**" SAE Paper 810233, 1981.

56. Hull D., "**Energy absorption of composite materials under crash conditions.**" *Progress in Science and Engineering of Composites*, Vol 1, pg 861-870.

57. Fairfull A.H. & Hull D., "**Effects of specimen dimensions on the specific energy absorption of fibre composite tubes.**" *ICCM IV & ECCM 2*, 1983, pg 3.36-3.45.

58. Wang A.S.D. & Crossman F.W., "**Calculation of edge stresses in multi-layer laminates by sub-structuring.**" *Journal of Composites Materials*, Vol 12, pg 76-83.

59. Han T.M., Hahn H.T. & Croman R.B., "**A Simplified Analysis of Transverse Ply Cracking in Cross-Ply Laminates.**" *Composites Science and Technology*., 1988, Vol 31, pg 165-177.

60. Chan W.S. & Wang A.S.D., "**Effects of a 90° on Matrix Cracks and Edge Delamination in Composite Laminates.**" *Composites Science and Technology*., 1990, Vol 38, pg 143-157.

61. Hamada H. & Ramakrishna S., "**Scaling Effects in the Energy Absorption of Carbon Fiber/PEEK Composite Tubes.**" *Composites Science and Technology*., 1995, Vol 55, pg 211-221.

62. Chan W.S. & Wang A.S.D., "**Fracture Mechanics.**" Chapter 4, pg 86.

63. Armanios E.A., "**Interlaminar Fracture in Graphite/Epoxy Composites.**" *Key Engineering Materials*, 1989, Vol 37, pg 85-102.

64. Gudmundson P., "**Fracture and Demage of Composite Laminates.**" *Engineering Mechanics of Fiber Reinforced Polymers and Composite Structures*., Chapter 5, pg 111-139.

65. Agarwal B.D. & Brontman L.J., "**Analysis and Performance of Fibre Composites.**" 2nd Edition, Chapter 7, pg 252.

66. Hamada H. & Ramakrishna S., "**Damage and Fracture of Fibre Composites.**" *Design with Advanced Composite Materials*., 1989, Chapter 10, pg 303.

67. Vinson J.R. & Chou T.W., "**Composite Materials and Their Use in Structure.**" Chapter 4 & Chapter 8.

68. Kim K.H., Shin K.C. & Lee J.J., " **Axial Crush and Energy Absorption Characteristics of Aluminium/GFRP Hybrid Square Tube.**", *Key Engineering Materials*, 2000, Vols 183-187, pg 1147-1152.

Appendices

Working for Crushing Stress (σ_c) calculation with Crack Length (a) varies from 1mm to 10mm.

C/PEEK (0°)

5mm → $$\sigma_c = \frac{2}{a\sin\theta}\sqrt{\frac{GEh}{3}} + \frac{\pi^2 Eh^2}{12l^2}\sec\theta$$

$$\sigma_c = \frac{2}{5x10^{-3}\sin 30°}\sqrt{\frac{1560(131x10^9)1.25x10^{-3}}{3}} + \frac{3.14^2(131x10^9)(1.25x10^{-3})^2}{12(55x10^{-3})^2}\frac{1}{\cos 30°}$$

= 297 x 10^6 Pascal

1mm → $\sigma_c = 1231 \times 10^6$ 2mm → $\sigma_c = 648 \times 10^6$

3mm → $\sigma_c = 453 \times 10^6$ 4mm → $\sigma_c = 356 \times 10^6$

6mm → $\sigma_c = 258 \times 10^6$ 7mm → $\sigma_c = 231 \times 10^6$

8mm → $\sigma_c = 210 \times 10^6$ 9mm → $\sigma_c = 194 \times 10^6$

10mm → $\sigma_c = 181 \times 10^6$

C/PEEK (30°)

5mm $\rightarrow$ $$\sigma_c = \frac{2}{a\sin\theta}\sqrt{\frac{GEh}{3}} + \frac{\pi^2 Eh^2}{12l^2}\sec\theta$$

$$\sigma_c = \frac{2}{5x10^{-3}\sin 30°}\sqrt{\frac{1560\left(65x10^9\right)1.25x10^{-3}}{3}} + \frac{3.14^2\left(65x10^9\right)\left(1.25x10^{-3}\right)^2}{12\left(55x10^{-3}\right)^2}\frac{1}{\cos 30°}$$

= 196 x 10^6 Pascal

1mm $\rightarrow$ σ_c = *854 x* 10^6 *2mm* $\rightarrow$ σ_c = *443 x* 10^6

3mm $\rightarrow$ σ_c = *306 x* 10^6 *4mm* $\rightarrow$ σ_c = *237 x* 10^6

6mm $\rightarrow$ σ_c = *169 x* 10^6 *7mm* $\rightarrow$ σ_c = *149 x* 10^6

8mm $\rightarrow$ σ_c = *134 x* 10^6 *9mm* $\rightarrow$ σ_c = *123 x* 10^6

10mm $\rightarrow$ σ_c = *114 x* 10^6

C/EPOXY (45°)

5mm $\rightarrow$ $$\sigma_c = \frac{2}{a\sin\theta}\sqrt{\frac{GEh}{3}} + \frac{\pi^2 Eh^2}{12l^2}\sec\theta$$

$$\sigma_c = \frac{2}{5x10^{-3}\sin 30°}\sqrt{\frac{120\left(66x10^9\right)1.25x10^{-3}}{3}} + \frac{3.14^2\left(66x10^9\right)\left(1.25x10^{-3}\right)^2}{12\left(55x10^{-3}\right)^2}\frac{1}{\cos 30°}$$

= 78 x 10^6 Pascal

1mm $\rightarrow$ σ_c = *262 x* 10^6 *2mm* $\rightarrow$ σ_c = *147 x* 10^6

3mm $\rightarrow$ σ_c = *109 x* 10^6 *4mm* $\rightarrow$ σ_c = *90 x* 10^6

6mm $\rightarrow$ σ_c = *71 x* 10^6 *7mm* $\rightarrow$ σ_c = *65 x* 10^6

8mm $\rightarrow$ σ_c = *61 x* 10^6 *9mm* $\rightarrow$ σ_c = *58 x* 10^6

10mm $\rightarrow$ σ_c = *55 x* 10^6

GL/CLOTH-EPOXY #1

5mm $\rightarrow$ $$\sigma_c = \frac{2}{a\sin\theta}\sqrt{\frac{GEh}{3}} + \frac{\pi^2 Eh^2}{12l^2}\sec\theta$$

$$\sigma_c = \frac{2}{5x10^{-3}\sin 30°}\sqrt{\frac{1207\left(21.4x10^9\right)1.25x10^{-3}}{3}} + \frac{3.14^2\left(21.4x10^9\right)\left(1.25x10^{-3}\right)^2}{12\left(55x10^{-3}\right)^2}\frac{1}{\cos 30°}$$

= 93 x 10^6 Pascal

1mm $\rightarrow$ σ_c = *425 x* 10^6 *2mm* $\rightarrow$ σ_c = *218 x* 10^6

3mm $\rightarrow$ σ_c = *149 x* 10^6 *4mm* $\rightarrow$ σ_c = *114 x* 10^6

6mm $\rightarrow$ σ_c = *80 x* 10^6 *7mm* $\rightarrow$ σ_c = *70 x* 10^6

8mm $\rightarrow$ σ_c = *62 x* 10^6 *9mm* $\rightarrow$ σ_c = *57 x* 10^6

10mm $\rightarrow$ σ_c = *52 x* 10^6

CL/CLOTH-EPOXY #2

5mm $\rightarrow$ $$\sigma_c = \frac{2}{a\sin\theta}\sqrt{\frac{GEh}{3}} + \frac{\pi^2 Eh^2}{12l^2}\sec\theta$$

$$\sigma_c = \frac{2}{5x10^{-3}\sin 30°}\sqrt{\frac{1196\left(20.9x10^9\right)1.25x10^{-3}}{3}} + \frac{3.14^2\left(20.9x10^9\right)\left(1.25x10^{-3}\right)^2}{12\left(55x10^{-3}\right)^2}\frac{1}{\cos 30°}$$

= 92 x 10^6 Pascal

1mm $\rightarrow$ $\sigma_c = 418 \times 10^6$ *2mm* $\rightarrow$ $\sigma_c = 214 \times 10^6$

3mm $\rightarrow$ $\sigma_c = 146 \times 10^6$ *4mm* $\rightarrow$ $\sigma_c = 112 \times 10^6$

6mm $\rightarrow$ $\sigma_c = 78 \times 10^6$ *7mm* $\rightarrow$ $\sigma_c = 69 \times 10^6$

8mm $\rightarrow$ $\sigma_c = 61 \times 10^6$ *9mm* $\rightarrow$ $\sigma_c = 56 \times 10^6$

10mm $\rightarrow$ $\sigma_c = 51 \times 10^6$

GL/CLOTH-EPOXY #3

5mm $\rightarrow$ $$\sigma_c = \frac{2}{a\sin\theta}\sqrt{\frac{GEh}{3}} + \frac{\pi^2 Eh^2}{12l^2}\sec\theta$$

$$\sigma_c = \frac{2}{5x10^{-3}\sin 30°}\sqrt{\frac{979\left(21.4x10^9\right)1.25x10^{-3}}{3}} + \frac{3.14^2\left(21.4x10^9\right)\left(1.25x10^{-3}\right)^2}{12\left(55x10^{-3}\right)^2}\frac{1}{\cos 30°}$$

= 85 x 10^6 Pascal

1mm $\rightarrow$ σ_c = *384 x* 10^6 *2mm* $\rightarrow$ σ_c = *197 x* 10^6

3mm $\rightarrow$ σ_c = *135 x* 10^6 *4mm* $\rightarrow$ σ_c = *104 x* 10^6

6mm $\rightarrow$ σ_c = *73 x* 10^6 *7mm* $\rightarrow$ σ_c = *64 x* 10^6

8mm $\rightarrow$ σ_c = *57 x* 10^6 *9mm* $\rightarrow$ σ_c = *52 x* 10^6

10mm $\rightarrow$ σ_c = *48 x* 10^6

GL/CLOTH-EPOXY #4

5mm $\rightarrow$ $$\sigma_c = \frac{2}{a\sin\theta}\sqrt{\frac{GEh}{3}} + \frac{\pi^2 Eh^2}{12l^2}\sec\theta$$

$$\sigma_c = \frac{2}{5x10^{-3}\sin 30°}\sqrt{\frac{1038\left(20x10^9\right)1.25x10^{-3}}{3}} + \frac{3.14^2\left(20x10^9\right)\left(1.25x10^{-3}\right)^2}{12\left(55x10^{-3}\right)^2}\frac{1}{\cos 30°}$$

= 84 x 10^6 Pascal

1mm $\rightarrow$ σ_c = *382 x* 10^6 *2mm* $\rightarrow$ σ_c = *196 x* 10^6

3mm $\rightarrow$ σ_c = *134 x* 10^6 *4mm* $\rightarrow$ σ_c = *103 x* 10^6

6mm $\rightarrow$ σ_c = *72 x* 10^6 *7mm* $\rightarrow$ σ_c = *63 x* 10^6

8mm $\rightarrow$ σ_c = *56 x* 10^6 *9mm* $\rightarrow$ σ_c = *51 x* 10^6

10mm $\rightarrow$ σ_c = *47 x* 10^6

C/PEEK (B16)

5mm $\rightarrow$ $\sigma_c = \frac{2}{a\sin\theta}\sqrt{\frac{GEh}{3}} + \frac{\pi^2 Eh^2}{12l^2}\sec\theta$

$$\sigma_c = \frac{2}{5x10^{-3}\sin 30°}\sqrt{\frac{1750\left(134x10^9\right)1.10x10^{-3}}{3}} + \frac{3.14^2\left(134x10^9\right)\left(1.10x10^{-3}\right)^2}{12\left(55x10^{-3}\right)^2}\frac{1}{\cos 30°}$$

= 285 x 10^6 Pascal

1mm $\rightarrow$ σ_c = *1224 x* 10^6 *2mm* $\rightarrow$ σ_c = *637 x* 10^6

3mm $\rightarrow$ σ_c = *441 x* 10^6 *4mm* $\rightarrow$ σ_c = *344 x* 10^6

6mm $\rightarrow$ σ_c = *246 x* 10^6 *7mm* $\rightarrow$ σ_c = *218 x* 10^6

8mm $\rightarrow$ σ_c = *197 x* 10^6 *9mm* $\rightarrow$ σ_c = *181 x* 10^6

10mm $\rightarrow$ σ_c = *168 x* 10^6

C/PEEK (N16)

5mm $\rightarrow$ $$\sigma_c = \frac{2}{a\sin\theta}\sqrt{\frac{GEh}{3}} + \frac{\pi^2 Eh^2}{12l^2}\sec\theta$$

$$\sigma_c = \frac{2}{5x10^{-3}\sin 30°}\sqrt{\frac{1750\left(134x10^9\right)1.045x10^{-3}}{3}} + \frac{3.14^2\left(134x10^9\right)\left(1.045x10^{-3}\right)^2}{12\left(55x10^{-3}\right)^2}\frac{1}{\cos 30°}$$

= 274 x 10^6 Pascal

1mm $\rightarrow$ σ_c = *1189 x* 10^6 *2mm* $\rightarrow$ σ_c = *617 x* 10^6

3mm $\rightarrow$ σ_c = *427 x* 10^6 *4mm* $\rightarrow$ σ_c = *332 x* 10^6

6mm $\rightarrow$ σ_c = *236 x* 10^6 *7mm* $\rightarrow$ σ_c = *209 x* 10^6

8mm $\rightarrow$ σ_c = *189 x* 10^6 *9mm* $\rightarrow$ σ_c = *173 x* 10^6

10mm $\rightarrow$ σ_c = *160 x* 10^6

C/PEEK (N20)

5mm $\rightarrow$ $$\sigma_c = \frac{2}{a\sin\theta}\sqrt{\frac{GEh}{3}} + \frac{\pi^2 Eh^2}{12l^2}\sec\theta$$

$$\sigma_c = \frac{2}{5x10^{-3}\sin 30°}\sqrt{\frac{1750\left(134x10^9\right)1.33x10^{-3}}{3}} + \frac{3.14^2\left(134x10^9\right)\left(1.33x10^{-3}\right)^2}{12\left(55x10^{-3}\right)^2}\frac{1}{\cos 30°}$$

= 332 x 10^6 Pascal

1mm $\rightarrow$ σ_c = *1364 x* 10^6 *2mm* $\rightarrow$ σ_c = *719 x* 10^6

3mm $\rightarrow$ σ_c = *504 x* 10^6 *4mm* $\rightarrow$ σ_c = *396 x* 10^6

6mm $\rightarrow$ σ_c = *289 x* 10^6 *7mm* $\rightarrow$ σ_c = *258 x* 10^6

8mm $\rightarrow$ σ_c = *235 x* 10^6 *9mm* $\rightarrow$ σ_c = *217 x* 10^6

10mm $\rightarrow$ σ_c = *203 x* 10^6

C/PEEK (L116)

5mm $\rightarrow$ $$\sigma_c = \frac{2}{a\sin\theta}\sqrt{\frac{GEh}{3}} + \frac{\pi^2 Eh^2}{12l^2}\sec\theta$$

$$\sigma_c = \frac{2}{5x10^{-3}\sin 30°}\sqrt{\frac{1750\left(134x10^9\right)1.07x10^{-3}}{3}} + \frac{3.14^2\left(134x10^9\right)\left(1.07x10^{-3}\right)^2}{12\left(55x10^{-3}\right)^2}\frac{1}{\cos 30°}$$

= 279 x 10^6 Pascal

1mm $\rightarrow$ σ_c = *1204 x* 10^6 *2mm* $\rightarrow$ σ_c = *626 x* 10^6

3mm $\rightarrow$ σ_c = *434 x* 10^6 *4mm* $\rightarrow$ σ_c = *337 x* 10^6

6mm $\rightarrow$ σ_c = *241 x* 10^6 *7mm* $\rightarrow$ σ_c = *213 x* 10^6

8mm $\rightarrow$ σ_c = *193 x* 10^6 *9mm* $\rightarrow$ σ_c = *176 x* 10^6

10mm $\rightarrow$ σ_c = *164 x* 10^6

Working for Crushing Stress (σ_c) calculation with Composite Thickness (h) varies from 1mm to 10mm.

C/PEEK (0°)

1mm → $$\sigma_c = \frac{2}{a\sin\theta}\sqrt{\frac{GEh}{3}} + \frac{\pi^2 Eh^2}{12l^2}\sec\theta$$

$$\sigma_c = \frac{2}{5x10^{-3}\sin 30°}\sqrt{\frac{1560\left(131x10^9\right)1.00x10^{-3}}{3}} + \frac{3.14^2\left(131x10^9\right)\left(1.00x10^{-3}\right)^2}{12\left(55x10^{-3}\right)^2}\frac{1}{\cos 30°}$$

= 250 x 10^6 Pascal

2mm → $\sigma_c = 459x10^6$ *3mm* → $\sigma_c = 730x10^6$

4mm → $\sigma_c = 1072x10^6$ *5mm* → $\sigma_c = 1490x10^6$

6mm → $\sigma_c = 1985x10^6$ *7mm* → $\sigma_c = 2557x10^6$

8mm → $\sigma_c = 3209x10^6$ *9mm* → $\sigma_c = 3941x10^6$

10mm → $\sigma_c = 4752x10^6$

C/PEEK (30°)

1mm $\rightarrow$ $$\sigma_c = \frac{2}{a\sin\theta}\sqrt{\frac{GEh}{3}} + \frac{\pi^2 Eh^2}{12l^2}\sec\theta$$

$$\sigma_c = \frac{2}{5x10^{-3}\sin 30°}\sqrt{\frac{1560\left(65x10^9\right)1.00x10^{-3}}{3}} + \frac{3.14^2\left(65x10^9\right)\left(1.00x10^{-3}\right)^2}{12\left(55x10^{-3}\right)^2}\frac{1}{\cos 30°}$$

= 167 x 10^6 Pascal

2mm $\rightarrow$ $\sigma_c = 289x10^6$ *3mm* $\rightarrow$ $\sigma_c = 437x10^6$

4mm $\rightarrow$ $\sigma_c = 619x10^6$ *5mm* $\rightarrow$ $\sigma_c = 836x10^6$

6mm $\rightarrow$ $\sigma_c = 1091x10^6$ *7mm* $\rightarrow$ $\sigma_c = 1384x10^6$

8mm $\rightarrow$ $\sigma_c = 1715x10^6$ *9mm* $\rightarrow$ $\sigma_c = 2086x10^6$

10mm $\rightarrow$ $\sigma_c = 2495x10^6$

C/EPOXY (45°)

1mm $\rightarrow$ $$\sigma_c = \frac{2}{a\sin\theta}\sqrt{\frac{GEh}{3}} + \frac{\pi^2 Eh^2}{12l^2}\sec\theta$$

$$\sigma_c = \frac{2}{5x10^{-3}\sin 30°}\sqrt{\frac{120\left(66x10^9\right)1.00x10^{-3}}{3}} + \frac{3.14^2\left(66x10^9\right)\left(1.00x10^{-3}\right)^2}{12\left(55x10^{-3}\right)^2}\frac{1}{\cos 30°}$$

= 62 x 10^6 Pascal

2mm $\rightarrow$ $\sigma_c = 141x10^6$ *3mm* $\rightarrow$ $\sigma_c = 257x10^6$

4mm $\rightarrow$ $\sigma_c = 412x10^6$ *5mm* $\rightarrow$ $\sigma_c = 607x10^6$

6mm $\rightarrow$ $\sigma_c = 843x10^6$ *7mm* $\rightarrow$ $\sigma_c = 1119x10^6$

8mm $\rightarrow$ $\sigma_c = 1436x10^6$ *9mm* $\rightarrow$ $\sigma_c = 1793x10^6$

10mm $\rightarrow$ $\sigma_c = 2192x10^6$

GL/CLOTH-EPOXY #1

1mm $\rightarrow$ $$\sigma_c = \frac{2}{a\sin\theta}\sqrt{\frac{GEh}{3}} + \frac{\pi^2 Eh^2}{12l^2}\sec\theta$$

$$\sigma_c = \frac{2}{5x10^{-3}\sin 30°}\sqrt{\frac{1207\left(21.4x10^9\right)1.00x10^{-3}}{3}} + \frac{3.14^2\left(21.4x10^9\right)\left(1.00x10^{-3}\right)^2}{12\left(55x10^{-3}\right)^2}\frac{1}{\cos 30°}$$

= 81 x 10^6 Pascal

2mm $\rightarrow$ $\sigma_c = 132x10^6$ *3mm* $\rightarrow$ $\sigma_c = 189x10^6$

4mm $\rightarrow$ $\sigma_c = 255x10^6$ *5mm* $\rightarrow$ $\sigma_c = 333x10^6$

6mm $\rightarrow$ $\sigma_c = 422x10^6$ *7mm* $\rightarrow$ $\sigma_c = 524x10^6$

8mm $\rightarrow$ $\sigma_c = 638x10^6$ *9mm* $\rightarrow$ $\sigma_c = 764x10^6$

10mm $\rightarrow$ $\sigma_c = 903x10^6$

CL/CLOTH-EPOXY #2

1mm $\rightarrow$ $$\sigma_c = \frac{2}{a\sin\theta}\sqrt{\frac{GEh}{3}} + \frac{\pi^2 Eh^2}{12l^2}\sec\theta$$

$$\sigma_c = \frac{2}{5x10^{-3}\sin 30°}\sqrt{\frac{1196\left(20.9x10^9\right)1.00x10^{-3}}{3}} + \frac{3.14^2\left(20.9x10^9\right)\left(1.00x10^{-3}\right)^2}{12\left(55x10^{-3}\right)^2}\frac{1}{\cos 30°}$$

= 80 x 10^6 Pascal

2mm $\rightarrow$ $\sigma_c = 129x10^6$ *3mm* $\rightarrow$ $\sigma_c = 185x10^6$

4mm $\rightarrow$ $\sigma_c = 251x10^6$ *5mm* $\rightarrow$ $\sigma_c = 326x10^6$

6mm $\rightarrow$ $\sigma_c = 414x10^6$ *7mm* $\rightarrow$ $\sigma_c = 513x10^6$

8mm $\rightarrow$ $\sigma_c = 624x10^6$ *9mm* $\rightarrow$ $\sigma_c = 748x10^6$

10mm $\rightarrow$ $\sigma_c = 884x10^6$

GL/CLOTH-EPOXY #3

1mm $\rightarrow$ $$\sigma_c = \frac{2}{a\sin\theta}\sqrt{\frac{GEh}{3}} + \frac{\pi^2 Eh^2}{12l^2}\sec\theta$$

$$\sigma_c = \frac{2}{5x10^{-3}\sin 30°}\sqrt{\frac{979\left(21.4x10^9\right)1.00x10^{-3}}{3}} + \frac{3.14^2\left(21.4x10^9\right)\left(1.00x10^{-3}\right)^2}{12\left(55x10^{-3}\right)^2}\frac{1}{\cos 30°}$$

= 74 x 10^6 Pascal

2mm $\rightarrow$ $\sigma_c = 121x10^6$ *3mm* $\rightarrow$ $\sigma_c = 176x10^6$

4mm $\rightarrow$ $\sigma_c = 241x10^6$ *5mm* $\rightarrow$ $\sigma_c = 317x10^6$

6mm $\rightarrow$ $\sigma_c = 373x10^6$ *7mm* $\rightarrow$ $\sigma_c = 504x10^6$

8mm $\rightarrow$ $\sigma_c = 617x10^6$ *9mm* $\rightarrow$ $\sigma_c = 742x10^6$

10mm $\rightarrow$ $\sigma_c = 880x10^6$

GL/CLOTH-EPOXY #4

1mm $\rightarrow$ $$\sigma_c = \frac{2}{a\sin\theta}\sqrt{\frac{GEh}{3}} + \frac{\pi^2 Eh^2}{12l^2}\sec\theta$$

$$\sigma_c = \frac{2}{5x10^{-3}\sin 30°}\sqrt{\frac{1038\left(20x10^9\right)1.00x10^{-3}}{3}} + \frac{3.14^2\left(20x10^9\right)\left(1.00x10^{-3}\right)^2}{12\left(55x10^{-3}\right)^2}\frac{1}{\cos 30°}$$

= 73 x 10^6 Pascal

2mm $\rightarrow$ $\sigma_c = 119x10^6$ *3mm* $\rightarrow$ $\sigma_c = 171x10^6$

4mm $\rightarrow$ $\sigma_c = 233x10^6$ *5mm* $\rightarrow$ $\sigma_c = 305x10^6$

6mm $\rightarrow$ $\sigma_c = 388x10^6$ *7mm* $\rightarrow$ $\sigma_c = 482x10^6$

8mm $\rightarrow$ $\sigma_c = 588x10^6$ *9mm* $\rightarrow$ $\sigma_c = 706x10^6$

10mm $\rightarrow$ $\sigma_c = 835x10^6$

Working for Crushing Stress (σ_c) calculation with Crack Opening Angle (θ) varies from 5° to 80º.

C/PEEK (0°)

5º → $$\sigma_c = \frac{2}{a\sin\theta}\sqrt{\frac{GEh}{3}} + \frac{\pi^2 Eh^2}{12l^2}\sec\theta$$

$$\sigma_c = \frac{2}{5x10^{-3}\sin 5°}\sqrt{\frac{1560\left(131x10^9\right)1.25x10^{-3}}{3}} + \frac{3.14^2\left(131x10^9\right)\left(1.25x10^{-3}\right)^2}{12\left(55x10^{-3}\right)^2}\frac{1}{\cos 5°}$$

= 1395 x 10^6 Pascal

10º → $\sigma_c = 729x10^6$ 20º → $\sigma_c = 400x10^6$

30º → $\sigma_c = 298x10^6$ 40º → $\sigma_c = 254x10^6$

50º → $\sigma_c = 239x10^6$ 60º → $\sigma_c = 246x10^6$

70º → $\sigma_c = 287x10^6$ 80º → $\sigma_c = 439x10^6$

C/PEEK (30°)

5° → $$\sigma_c = \frac{2}{a\sin\theta}\sqrt{\frac{GEh}{3}} + \frac{\pi^2 Eh^2}{12l^2}\sec\theta$$

$$\sigma_c = \frac{2}{5x10^{-3}\sin 5°}\sqrt{\frac{1560\left(65x10^9\right)1.25x10^{-3}}{3}} + \frac{3.14^2\left(65x10^9\right)\left(1.25x10^{-3}\right)^2}{12\left(55x10^{-3}\right)^2}\frac{1}{\cos 5°}$$

= 971 x 10^6 Pascal

10° → $\sigma_c = 501x10^6$ 20° → $\sigma_c = 270x10^6$

30° → $\sigma_c = 196x10^6$ 40° → $\sigma_c = 164x10^6$

50° → $\sigma_c = 150x10^6$ 60° → $\sigma_c = 150x10^6$

70° → $\sigma_c = 168x10^6$ 80° → $\sigma_c = 242x10^6$

C/EPOXY (45°)

5º → $\sigma_c = \frac{2}{a\sin\theta}\sqrt{\frac{GEh}{3}} + \frac{\pi^2 Eh^2}{12l^2}\sec\theta$

$$\sigma_c = \frac{2}{5x10^{-3}\sin 5°}\sqrt{\frac{120\left(66x10^9\right)1.25x10^{-3}}{3}} + \frac{3.14^2\left(66x10^9\right)\left(1.25x10^{-3}\right)^2}{12\left(55x10^{-3}\right)^2}\frac{1}{\cos 5°}$$

= 292 x 10^6 Pascal

10º → $\sigma_c = 160x10^6$ 20º → $\sigma_c = 97x10^6$

30º → $\sigma_c = 78x10^6$ 40º → $\sigma_c = 72x10^6$

50º → $\sigma_c = 74x10^6$ 60º → $\sigma_c = 83x10^6$

70º → $\sigma_c = 106x10^6$ 80º → $\sigma_c = 185x10^6$

CL/CLOTH-EPOXY #1

5º → $$\sigma_c = \frac{2}{a\sin\theta}\sqrt{\frac{GEh}{3}} + \frac{\pi^2 Eh^2}{12l^2}\sec\theta$$

$$\sigma_c = \frac{2}{5x10^{-3}\sin 5°}\sqrt{\frac{1207\left(21.4x10^{9}\right)1.25x10^{-3}}{3}} + \frac{3.14^2\left(21.4x10^{9}\right)\left(1.25x10^{-3}\right)^2}{12\left(55x10^{-3}\right)^2}\frac{1}{\cos 5°}$$

= 485 x 10^6 Pascal

10º → $\sigma_c = 248x10^6$ 20º → $\sigma_c = 131x10^6$

30º → $\sigma_c = 93x10^6$ 40º → $\sigma_c = 76x10^6$

50º → $\sigma_c = 68x10^6$ 60º → $\sigma_c = 66x10^6$

70º → $\sigma_c = 71x10^6$ 80º → $\sigma_c = 94x10^6$

CL/CLOTH-EPOXY #2

5º → $$\sigma_c = \frac{2}{a\sin\theta}\sqrt{\frac{GEh}{3}} + \frac{\pi^2 Eh^2}{12l^2}\sec\theta$$

$$\sigma_c = \frac{2}{5x10^{-3}\sin 5°}\sqrt{\frac{1196\left(20.9x10^9\right)1.25x10^{-3}}{3}} + \frac{3.14^2\left(20.9x10^9\right)\left(1.25x10^{-3}\right)^2}{12\left(55x10^{-3}\right)^2}\frac{1}{\cos 5°}$$

= 477 x 10^6 Pascal

10º → $\sigma_c = 244x10^6$ 20º → $\sigma_c = 129x10^6$

30º → $\sigma_c = 92x10^6$ 40º → $\sigma_c = 75x10^6$

50º → $\sigma_c = 67x10^6$ 60º → $\sigma_c = 65x10^6$

70º → $\sigma_c = 69x10^6$ 80º → $\sigma_c = 93x10^6$

CL/CLOTH-EPOXY #3

5º → $$\sigma_c = \frac{2}{a\sin\theta}\sqrt{\frac{GEh}{3}} + \frac{\pi^2 Eh^2}{12l^2}\sec\theta$$

$$\sigma_c = \frac{2}{5x10^{-3}\sin 5°}\sqrt{\frac{979\left(21.4x10^{9}\right)1.25x10^{-3}}{3}} + \frac{3.14^2\left(21.4x10^{9}\right)\left(1.25x10^{-3}\right)^2}{12\left(55x10^{-3}\right)^2}\frac{1}{\cos 5°}$$

= 438 x 10^6 Pascal

10º → $\sigma_c = 224x10^6$ 20º → $\sigma_c = 119x10^6$

30º → $\sigma_c = 85x10^6$ 40º → $\sigma_c = 70x10^6$

50º → $\sigma_c = 63x10^6$ 60º → $\sigma_c = 61x10^6$

70º → $\sigma_c = 66x10^6$ 80º → $\sigma_c = 90x10^6$

CL/CLOTH-EPOXY #4

5º → $\sigma_c = \frac{2}{a \sin\theta}\sqrt{\frac{GEh}{3}} + \frac{\pi^2 Eh^2}{12l^2}\sec\theta$

$$\sigma_c = \frac{2}{5x10^{-3}\sin 5°}\sqrt{\frac{1038\left(20x10^9\right)1.25x10^{-3}}{3}} + \frac{3.14^2\left(20x10^9\right)\left(1.25x10^{-3}\right)^2}{12\left(55x10^{-3}\right)^2}\frac{1}{\cos 5°}$$

= 435 x 10^6 Pascal

10º → $\sigma_c = 223x10^6$ 20º → $\sigma_c = 118x10^6$

30º → $\sigma_c = 84x10^6$ 40º → $\sigma_c = 69x10^6$

50º → $\sigma_c = 62x10^6$ 60º → $\sigma_c = 60x10^6$

70º → $\sigma_c = 64x10^6$ 80º → $\sigma_c = 87x10^6$

Working for Energy Release Rate (G) calculation using the calculated Crushing Stress (σ_c) with Crack Length fixed at 5mm.

C/PEEK(0º)

$$G = \frac{3(a\sin\theta)^2}{Eh}\left(\frac{\sigma_c}{2} - \frac{\pi^2 Eh^2 \sec\theta}{24l^2}\right)^2$$

$$G = \frac{3\left(5x10^{-3}\sin 30°\right)^2}{131x10^9\left(1.25x10^{-3}\right)}\left(\frac{297x10^6}{2} - \frac{3.14^2\left(131x10^9\right)\left(1.25x10^{-3}\right)^2\frac{1}{\cos 30°}}{24\left(55x10^{-3}\right)^2}\right)^2$$

= 1551 N/m

C/PEEK(30º)

$$G = \frac{3(a\sin\theta)^2}{Eh}\left(\frac{\sigma_c}{2} - \frac{\pi^2 Eh^2 \sec\theta}{24l^2}\right)^2$$

$$G = \frac{3\left(5x10^{-3}\sin 30°\right)^2}{65x10^9\left(1.25x10^{-3}\right)}\left(\frac{196x10^6}{2} - \frac{3.14^2\left(65x10^9\right)\left(1.25x10^{-3}\right)^2\frac{1}{\cos 30°}}{24\left(55x10^{-3}\right)^2}\right)^2$$

= 1554 N/m

C/EPOXY(45º)

$$G = \frac{3(a\sin\theta)^2}{Eh}\left(\frac{\sigma_c}{2} - \frac{\pi^2 Eh^2 \sec\theta}{24l^2}\right)^2$$

$$G = \frac{3\left(5x10^{-3}\sin 30°\right)^2}{66x10^9\left(1.25x10^{-3}\right)}\left(\frac{78x10^6}{2} - \frac{3.14^2\left(66x10^9\right)\left(1.25x10^{-3}\right)^2\frac{1}{\cos 30°}}{24\left(55x10^{-3}\right)^2}\right)^2$$

= 118 N/m

GL/CLOTH-EPOXY #1

$$G = \frac{3(a\sin\theta)^2}{Eh}\left(\frac{\sigma_c}{2} - \frac{\pi^2 Eh^2 \sec\theta}{24l^2}\right)^2$$

$$G = \frac{3\left(5x10^{-3}\sin 30°\right)^2}{21.4x10^9\left(1.25x10^{-3}\right)}\left(\frac{93x10^6}{2} - \frac{3.14^2\left(21.4x10^9\right)\left(1.25x10^{-3}\right)^2\frac{1}{\cos 30°}}{24\left(55x10^{-3}\right)^2}\right)^2$$

= 1193 N/m

GL-CLOTH-EPOXY #2

$$G = \frac{3(a\sin\theta)^2}{Eh}\left(\frac{\sigma_c}{2} - \frac{\pi^2 Eh^2 \sec\theta}{24l^2}\right)^2$$

$$G = \frac{3\left(5x10^{-3}\sin 30°\right)^2}{20.9x10^9\left(1.25x10^{-3}\right)}\left(\frac{92x10^6}{2} - \frac{3.14^2\left(20.9x10^9\right)\left(1.25x10^{-3}\right)^2\frac{1}{\cos 30°}}{24\left(55x10^{-3}\right)^2}\right)^2$$

= 1485 N/m

GL/CLOTH-EPOXY #3

$$G = \frac{3(a\sin\theta)^2}{Eh}\left(\frac{\sigma_c}{2} - \frac{\pi^2 Eh^2 \sec\theta}{24l^2}\right)^2$$

$$G = \frac{3\left(5x10^{-3}\sin 30°\right)^2}{21.4x10^9\left(1.25x10^{-3}\right)}\left(\frac{85x10^6}{2} - \frac{3.14^2\left(21.4x10^9\right)\left(1.25x10^{-3}\right)^2\frac{1}{\cos 30°}}{24\left(55x10^{-3}\right)^2}\right)^2$$

= 973 N/m

GL-CLOTH-EPOXY #4

$$G = \frac{3(a\sin\theta)^2}{Eh}\left(\frac{\sigma_c}{2} - \frac{\pi^2 Eh^2 \sec\theta}{24l^2}\right)^2$$

$$G = \frac{3\left(5x10^{-3}\sin 30°\right)^2}{20.9x10^9\left(1.25x10^{-3}\right)}\left(\frac{84x10^6}{2} - \frac{3.14^2\left(20.9x10^9\right)\left(1.25x10^{-3}\right)^2\frac{1}{\cos 30°}}{24\left(55x10^{-3}\right)^2}\right)^2$$

= 1032 N/m

C/PEEK (B16)

$$G = \frac{3(a\sin\theta)^2}{Eh}\left(\frac{\sigma_c}{2} - \frac{\pi^2 Eh^2 \sec\theta}{24l^2}\right)^2$$

$$G = \frac{3\left(5x10^{-3}\sin 30°\right)^2}{134x10^9\left(1.10x10^{-3}\right)}\left(\frac{285x10^6}{2} - \frac{3.14^2\left(134x10^9\right)\left(1.10x10^{-3}\right)^2\frac{1}{\cos 30°}}{24\left(55x10^{-3}\right)^2}\right)^2$$

= 1746 N/m

C/PEEK (N16)

$$G = \frac{3(a\sin\theta)^2}{Eh}\left(\frac{\sigma_c}{2} - \frac{\pi^2 Eh^2 \sec\theta}{24l^2}\right)^2$$

$$G = \frac{3\left(5x10^{-3}\sin 30°\right)^2}{134x10^9\left(1.045x10^{-3}\right)}\left(\frac{274x10^6}{2} - \frac{3.14^2\left(134x10^9\right)\left(1.045x10^{-3}\right)^2\frac{1}{\cos 30°}}{24\left(55x10^{-3}\right)^2}\right)^2$$

= 1744 N/m

C/PEEK (N20)

$$G = \frac{3(a\sin\theta)^2}{Eh}\left(\frac{\sigma_c}{2} - \frac{\pi^2 Eh^2 \sec\theta}{24l^2}\right)^2$$

$$G = \frac{3\left(5x10^{-3}\sin 30°\right)^2}{134x10^9\left(1.33x10^{-3}\right)}\left(\frac{332x10^6}{2} - \frac{3.14^2\left(134x10^9\right)\left(1.33x10^{-3}\right)^2\frac{1}{\cos 30°}}{24\left(55x10^{-3}\right)^2}\right)^2$$

= 1750 N/m

C/PEEK (L116)

$$G = \frac{3(a\sin\theta)^2}{Eh}\left(\frac{\sigma_c}{2} - \frac{\pi^2 Eh^2 \sec\theta}{24l^2}\right)^2$$

$$G = \frac{3\left(5x10^{-3}\sin 30°\right)^2}{134x10^9\left(1.07x10^{-3}\right)}\left(\frac{279x10^6}{2} - \frac{3.14^2\left(134x10^9\right)\left(1.07x10^{-3}\right)^2\dfrac{1}{\cos 30°}}{24\left(55x10^{-3}\right)^2}\right)^2$$

= 1746 N/m

Figure 5.1 :Crush Stress Versu Crack Length

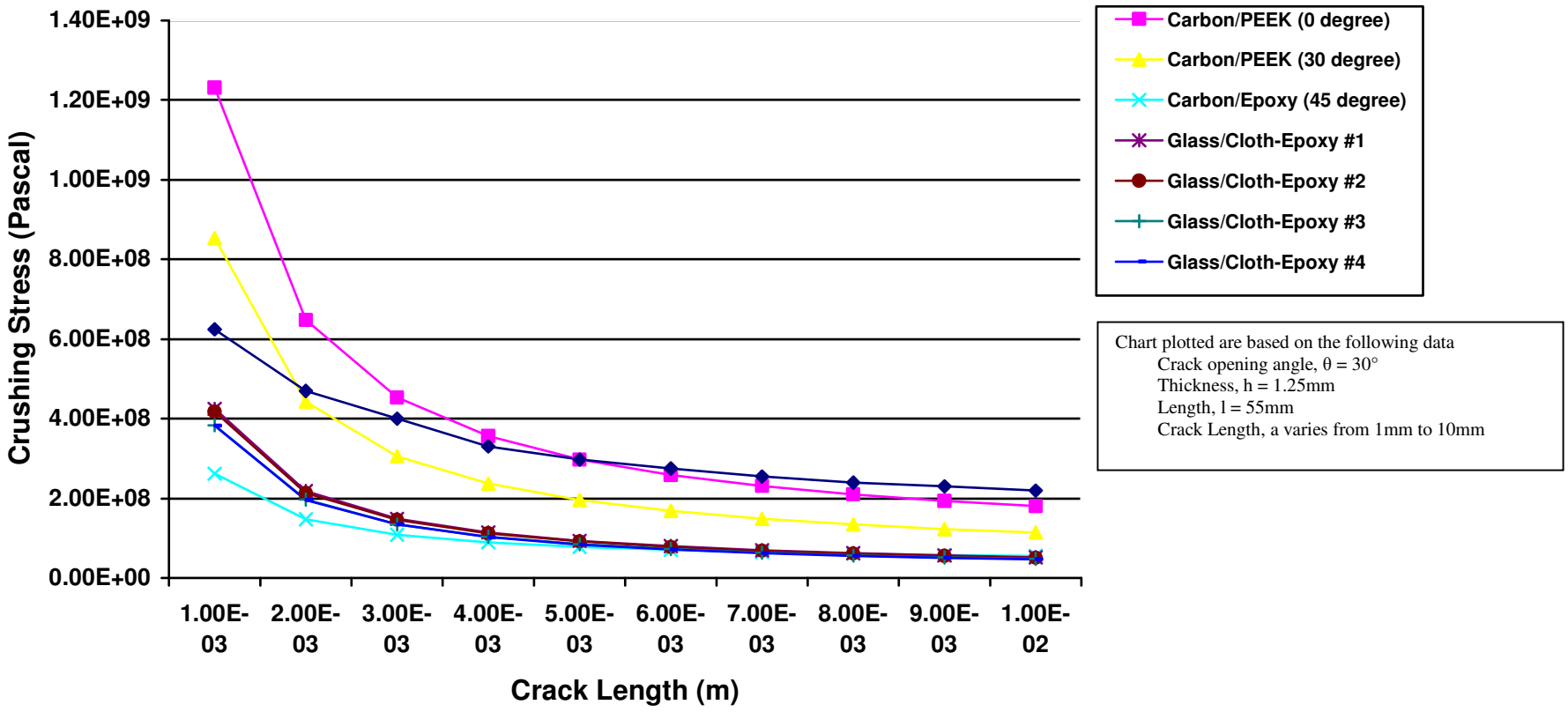

Figure 5.2 :Crush Stress Versu Composite Thickness

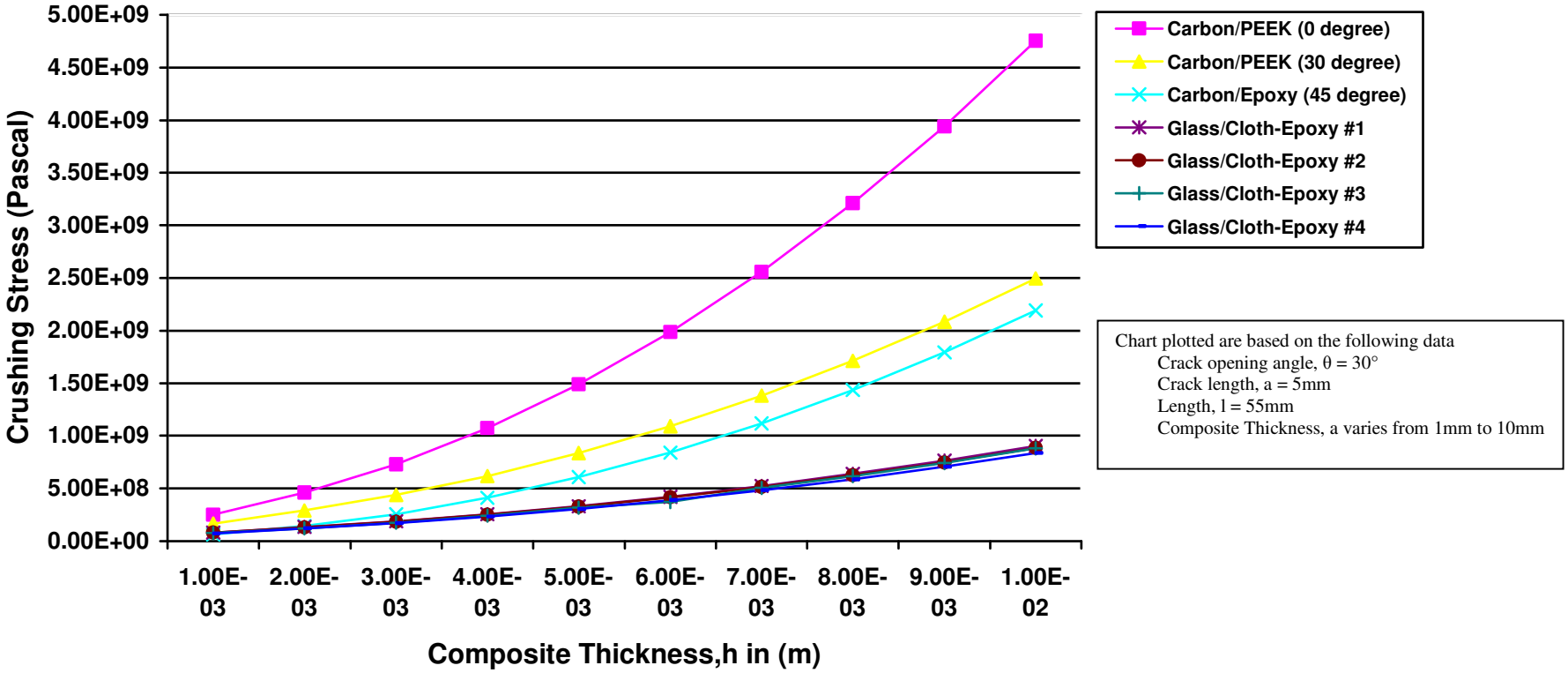

Chart plotted are based on the following data
- Crack opening angle, θ = 30°
- Crack length, a = 5mm
- Length, l = 55mm
- Composite Thickness, a varies from 1mm to 10mm

Figure 5.3 :Crush Stress Versu Crack Opening Angle

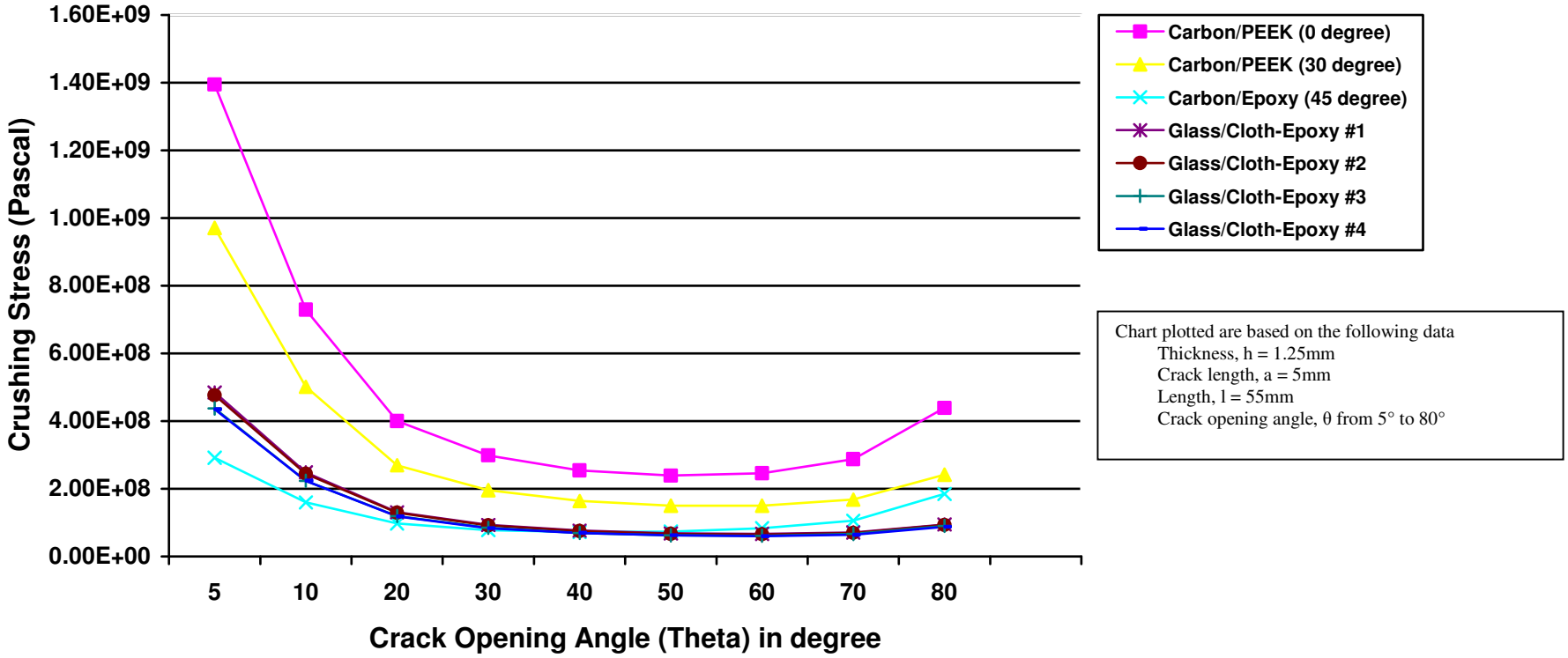

Figure 5.4 :Mean Crushing Load Versu Composite Thickness Experimental Data from Ref [68]

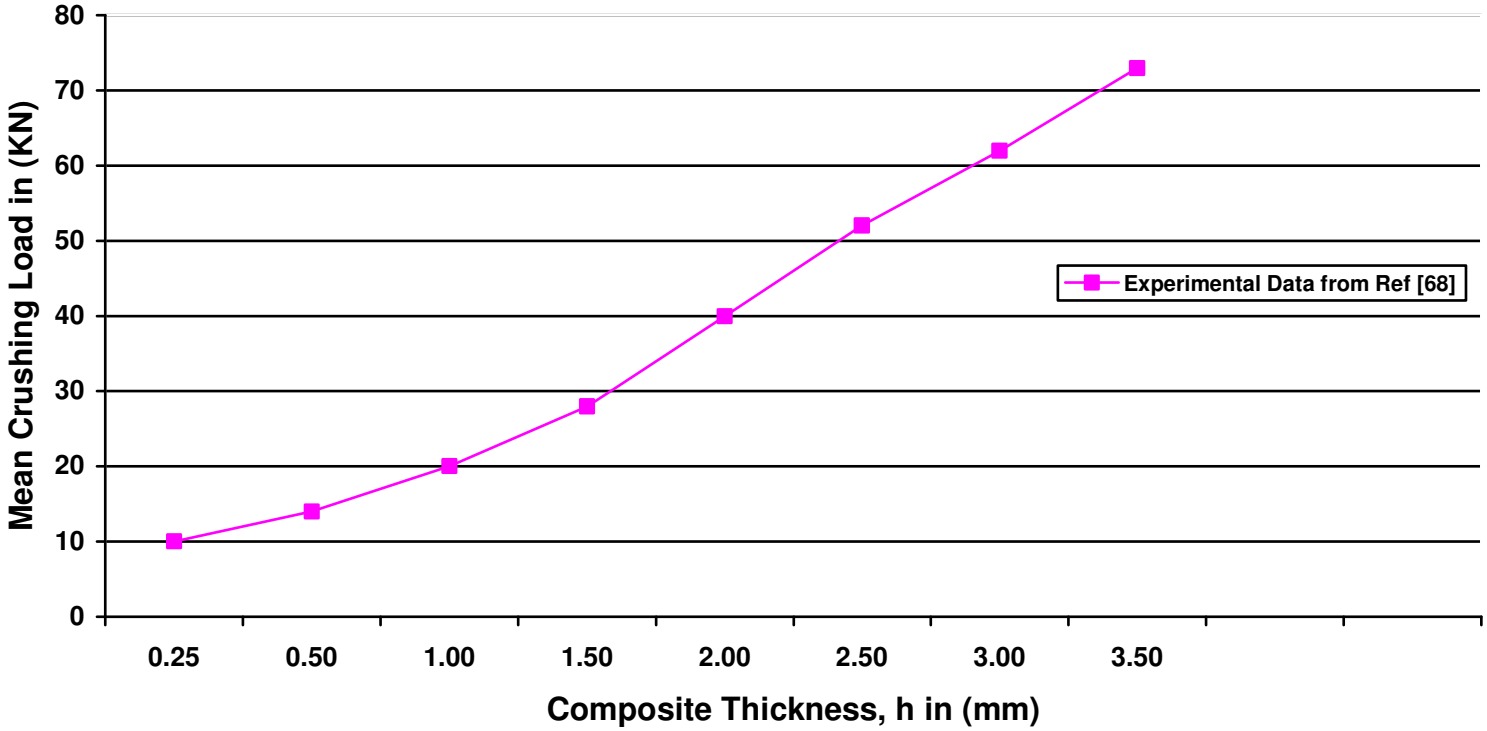

Project Timelines

S/NO	TASK	DURATION	START	FINISH
1	***Pre Project Planning***	60 Days	22 Dec 05	20 Feb 06
2	Project Proposal Submission	3 Days	16 Dec 05	18 Dec 05
3	Project Proposal Acceptance	11 Days	18 Dec 05	28 Dec 05
4	***Project Research***	60 Days	20 Feb 06	20 Apr 06
5	Research Information	19 Days	20 Feb 06	10 Mar 06
6	Compilation of Research Papers	15 Days	11 Mar 06	25 Mar 06
7	Reading up of Research Papers	20 Days	03 Apr 06	22 Apr 06
8	Additional Research if necessary	Cannot firm timeline due to uncertainty		
9	***Reports***			
10	Project Specification Writing	11 Days	15 Mar 06	25 Mar 06
11	Project Appreciation Writing	28 Days	17 April 06	14 May 06
12	First draft of Project Dissertation	60 Days	20 Apr 06	17 Jun 06
13	Final draft of Project Dissertation	80 Days	03 Aug 06	25 Oct 06
14	Documenting relevant information and drafting final Report	100 Days	16 Jul 06	25 Oct 06
15	Conclusion and recommendation for future work	20 Days	06 Oct 06	25 Oct 06
16	***Residential School***			
17	Meeting up with Supervisor	12 Days	25 Sep 06	06 Oct 06
18	Discussion with Supervisor on improvements for Project	12 Days	25 Sep 06	06 Oct 06

University of Southern Queensland

FACULTY OF ENGINEERING AND SURVEYING

ENG 4111/4112 Research Project
PROJECT SPECIFICATIONS

For: **Ang Soon Lim**

Topic: PREDICTING THE CRUSHING STRESS OF COMPOSITE MATERIALS

Supervisor: Dr Harry Ku

Co-Supervisor: Steven Goh

Sponsorship: Faculty of Engineering and Surveying, USQ

Project Aim: The objective of this project is to model the bearing failure of the composite joint with that of progressive crushing. A simple mathematical model for predicting the crushing stress of the composite materials is presented in this project. The present knowledge of fracture mechanics and strength of materials are used as a basis for the modeling process.

PROGRAMME : **Issue B, 22 March 2006**

1. Use USQ library online database and other Internet resources/tools to collect research papers, documents, standards, journal articles and book chapters.
2. Understand the concepts of fracture mechanics and strength of materials.
3. Review of previous works on Crushing Behaviour and Specific Energy Absorption.
4. To derive equation base Buckling Theory and Energy release rate (G) using Mode 1 failure to calculated required stresses.
5. To compare the calculated stresses with experimental data from technical and research papers.

As time permits

6. To implement a program using software such as Mathlab for easy calculation and comparison of data by other user.
7. To evaluate the derived equation with different modes of failure.

AGREED: _____(Student)_____,_____(Supervisor, Co-Supervisor)

___/___/___ ___/___/___ ___/___/___